Three-Dimensional Structure of Full-Length NtrX, an Unusual Member of the NtrC Family of Response Regulators

Ignacio Fernández[1,†], Irina Cornaciu[2,†], Mariela del Carmen Carrica[1], Emiko Uchikawa[2], Guillaume Hoffmann[2], Rodrigo Sieira[1], José Antonio Márquez[2] and Fernando A. Goldbaum[1]

*1 - **Fundación Instituto Leloir,** IIBBA-CONICET, Patricias Argentinas 435, C1405BWE Buenos Aires, Argentina*
*2 - **European Molecular Biology Laboratory (EMBL),** Grenoble Outstation, 71 Avenue des Martyrs, 38042 Grenoble, France*

***Correspondence to Fernando A. Goldbaum:** Av. Patricias Argentinas 435 (C1405BWE) Buenos Aires, Argentina.*
fgoldbaum@leloir.org.ar
http://dx.doi.org/10.1016/j.jmb.2016.12.022
Edited by Georg Schulz

Abstract

Bacteria sense and adapt to environmental changes using two-component systems. These signaling pathways are formed by a histidine kinase that phosphorylates a response regulator (RR), which finally modulates the transcription of target genes.

The bacterium *Brucella abortus* codes for a two-component system formed by the histidine kinase NtrY and the RR NtrX that participates in sensing low oxygen tension and generating an adaptive response. NtrX is a modular protein with REC, AAA+, and DNA-binding domains, an architecture that classifies it among the NtrC subfamily of RRs. However, it lacks the signature GAFTGA motif that is essential for activating transcription by the mechanism proposed for canonical members of this subfamily. In this article, we present the first crystal structure of full-length NtrX, which is also the first structure of a full-length NtrC-like RR with all the domains solved, showing that the protein is structurally similar to other members of the subfamily.

We also report that NtrX binds nucleotides and the structures of the protein bound to ATP and ADP. Despite binding ATP, NtrX does not have ATPase activity and does not form oligomers in response to phosphorylation or nucleotide binding. We also identify a nucleotide sequence recognized by NtrX that allows it to bind to a promoter region that regulates its own transcription and to establish a negative feedback mechanism to modulate its expression. Overall, this article provides a detailed description of the NtrX RR and supports that it functions by a mechanism different to classical NtrC-like RRs.

Introduction

Bacteria need to sense fluctuating environmental conditions and respond adequately in order to survive. For this, microbes use signaling pathways known as two-component systems (TCSs), which are formed by a histidine kinase (HK) and a response regulator (RR). Upon detection of a specific signal, the HK autophosphorylates and then transfers the phosphoryl group to the RR. The phosphorylated RR is activated to perform an output response that involves, in most cases, binding to DNA and modulating gene transcription [1].

TCSs are of particular importance in pathogenic bacteria such as *Brucella spp.* since they are a key factor for allowing bacteria to adapt to harsh conditions during the infection process. *Brucella* is the causative agent of brucellosis, one of the most important zoonotic diseases worldwide, causing abortion and sterility in domestic animals and undulant fever in humans [2]. *Brucella* codes for a TCS formed by the HK NtrY and the RR NtrX that participates in sensing low oxygen tension and in the adaptive response generated by activating the expression of denitrification enzymes and high-oxygen-affinity cytochrome oxidases [3,4]. The NtrY/X TCS is also present in other microorganisms and it has been involved in a variety of functions. These include nitrogen fixation and metabolism in *Azorhizobium caulinodans* [5]; inhibition of lysosomal fusion and

regulation of proline and glutamine metabolism in *Ehrlichia chaffeensis* [6,7]; expression of respiratory enzymes in *Neisseria gonorrhoeae* [8]; and succinoglycan production, motility, and symbiotic nodulation in *Sinorhizobium meliloti* [9]. It is noteworthy that *ntrX* was reported to be conditionally essential for *Caulobacter crescentus* [10].

NtrX is predicted to have three domains: (1) an N-terminal REC domain, (2) a central AAA+ (ATPases associated with various cellular activities) domain, and (3) a C-terminal DNA-binding domain (DBD) with a predicted helix-turn-helix (HTH) motif (Fig. SI1). Such architecture indicates that NtrX belongs to a subfamily of RRs in which the most extensively characterized member is NtrC [1]. Besides, some microorganisms (including *Brucella abortus*) code for NtrX in the same transcriptional unit as NtrC. Other members of the NtrC subfamily are *Aquifex aeolicus* NtrC1 and NtrC4, and *S. meliloti* DctD. These RRs act as bacterial enhancer-binding proteins (bEBPs), which are transcriptional regulators that activate the expression of σ^{54}-dependent genes. The postulated mechanism to explain the activation of NtrC-like RRs proposes that upon phosphorylation, these proteins form hexamers that hydrolyze ATP and couple the released energy with conformational changes that allow them to interact differentially with the σ^{54} factor of the RNA polymerase and initiate the transcription of target genes [11]. In these modular proteins, the N-terminal REC domain regulates the activity of the protein, while the central AAA+ domain participates in nucleotide binding, hydrolysis, oligomerization, and σ^{54} contact. In all the reported cases, the phosphorylation of the REC domain controls the AAA+ oligomerization, either promoting the formation of an oligomer (as in NtrC) or disrupting repressive interactions between the regulatory and central domains that leads to hexamerization (as in NtrC1 and DctD) [11]. The analysis of NtrX sequence indicates that several motifs of the AAA+ domain [11,12] are conserved (Fig. SI1). Some examples are the Walker A motif and the Sensor II that usually participate in ATP binding, the Walker B motif and arginine fingers that are involved in nucleotide hydrolysis, and the Sensor I that couples ATP hydrolysis with conformational changes linked to transcriptional activation. However, NtrX has not conserved a GAFTGA motif, considered a bEBP-specific structural element whose mutations produce severe defects in the ability to contact σ^{54} or activate transcription [11] (Fig. SI1). In some bacterial species (like *B. abortus*), the corresponding sequence in NtrX has been deleted; meanwhile, in other microorganisms, the sequence is present, but it has not been conserved (Fig. SI2). Some NtrC-like RRs that lack a functional GAFTGA, such as *Rhodobacter capsulatus* NtrC and HupR, have been classified in an unusual group that regulates transcription at σ^{70} promoters [13,14].

Despite all the knowledge regarding the cellular processes regulated by NtrX that was generated by genetic approaches in different microorganisms, little structural and biochemical information is available on how the RR functions. Our group has previously reported the structures of a truncated construct of NtrX REC domain in its apo state and bound to beryllofluoride (BeF_3^-) [15]. However, structural information on full-length NtrX that could provide details about the organization and interplay between the three domains is still lacking. In this article, we present the structure of NtrX in its apo and nucleotide-bound forms, obtained through X-ray crystallography, showing for the first time the architecture and relative organization of the REC, AAA+, and DBDs. This represents not only the first structure of an NtrX ortholog but also the first structure of a full-length NtrC-like RR with all the domains solved. Our results indicate that NtrX is structurally similar to *A. aeolicus* NtrC1 and NtrC4, but unlike them, it is not able to hydrolyze ATP or form oligomers. Moreover, we identified a nucleotide sequence recognized by NtrX that allows it to bind to a promoter region that regulates its own transcription, and we demonstrated that NtrX acts as a repressor at this promoter, establishing a negative feedback mechanism to modulate its expression. Overall, our results provide a detailed description of the NtrX RR and support that it functions by a mechanism different to classical bEBPs.

Results

NtrX crystal structure—overall description

In order to determine the structure of an NtrX ortholog, we cloned and expressed the full-length sequence of NtrX from *B. abortus*. The purified protein was crystallized through the integrated crystallization pipeline of the High Throughput Crystallization Laboratory of the EMBL Grenoble Outstation, including the steps of screening, optimization of crystal conditions, and automated crystal mounting and cryo-cooling using the CrystalDirect™ Technology [16]. The resulting crystals were analyzed for diffraction at the macromolecular crystallography beamlines of the ESRF. Several crystal forms for apo NtrX were identified, and one of them showed diffraction to a resolution of 2.2 Å in the orthorhombic space group $C222_1$. The final structure was solved from a native dataset by experimental phasing using crystals derivatized with ytterbium (Fig. 1a and Table 1).

Two chains were found in the asymmetric unit (A, B) with an RMSD value of 0.90 Å (378 residues aligned), forming a dimer with a buried surface area (BSA) of 9000 $Å^2$. The electron density maps

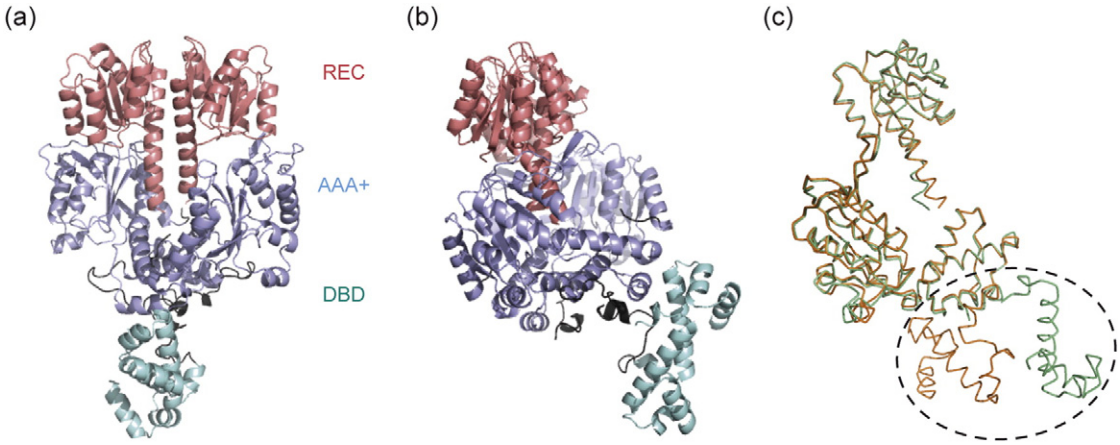

Fig. 1. NtrX crystal structure. (a) Structure of NtrX represented in cartoon, with its three domains in different colors (REC, pink; AAA+, light blue; DBD, green). (b) Side view of the NtrX structure. (c) Superposition of the two chains found in the asymmetric unit (A, orange; B, green) with a dashed-line oval to highlight the asymmetry in the C-terminal helices.

allowed tracing almost the complete backbone and side chains of each one, except residues 137–141 in chain A, and residues 136–142 and 389–399 in chain B. The three domains can be clearly observed in the crystallographic structure (Fig. 1a and b). The REC domain corresponds to residues 1–135 and presents an α/β topology, as has been previously reported for a truncated construct (PDB 4D6X) [15], with an RMSD of 0.60 Å between both structures. A long linker (linker 1, residues 136–146) connects the REC domain to the AAA+ domain, and its structure could not be modeled due to low electron density, possibly as a consequence of high flexibility in this region. The AAA+ domain includes residues 147–369 and is formed by an N-terminal α/β subdomain and a C-terminal helical subdomain, in accordance with other crystallographic structures reported for other AAA+ domains [12]. Another long linker (linker 2, residues 370–399) connects the central domain to the DBD (residues 400–451). The structure of this loop could be determined for chain A, possibly due to the presence of some interactions that reduce flexibility (E386-R364′, D341-Q400′, G388-H401′), but the electron density corresponding to most of the residues in chain B was absent.

The DBD presents an HTH motif formed by four helices: A (dimer buttress), B (dimerization helix), C (first helix of the HTH), and D (recognition helix, which typically binds to the major groove in the DNA) [17] (Fig. SI3a). In the case of NtrX, the dimer buttress helix is very short (four residues), as has been reported for NtrC4 (Fig. SI3b) [18]. As has been mentioned above, NtrX crystallized as a dimer in which the superposition of both chains resulted very well for residues comprising the REC and AAA+ domains. However, the C-terminal helices could not be aligned (Fig. 1c), and therefore, the orientation of the dimeric DBD introduced asymmetry in the overall structure of the protein.

NtrX resembles the general arrangement of typical NtrC-like RRs

A PDBeFold server search [19] revealed that the best fits for NtrX correspond to the RRs NtrC1 and NtrC4 from *A. aeolicus*, which also belong to the NtrC subfamily. Two structures are available for NtrC1: one of them was obtained using a full-length construct, but only weak and diffuse density was observable in the region corresponding to the DBD, so it was not possible to interpret any of that density with a structural model (PDB 4L4U); the other structure corresponds to a REC-AAA construct crystallized with ADP (PDB 1NY5). Also, a REC-AAA construct was crystallized in the presence of ADP to solve the structure of NtrC4 (PDB 3DZD). Therefore, in this article, we are presenting not only the first structure of an NtrX ortholog but also the first structure of a full-length NtrC-like RR with all the domains solved. Comparison between NtrX and NtrC1 or NtrC4 reveals that the REC and AAA+ domains have the same general arrangement, showing that the three proteins form homodimers with contacts between each domain (REC-REC, AAA-AAA, and REC-AAA), generating a similar overall structure (Fig. SI4a–c). Like NtrC1, and in contrast to NtrC4 that has a short unstructured connector, NtrX preserves the C-terminal portion of the long α5 helix from the REC domain. The structural alignments of individual REC and AAA+ domains from NtrX with those of NtrC1 have RMSD values close to 1.25 Å and 1.50 Å, respectively. However, the whole REC-AAA chains do not align so well (RMSD around 3.90 Å) because of the relative orientations of the REC and AAA+ domains.

Table 1. Data collection and refinement statistics

Statistics		NtrX	NtrX -ATP	NtrX -ADP
PDB code		5M7O	5M7N	5M7P
Data collection				
Synchrotron source		ESRF	ESRF	ESRF
Beamline		ID29	MASSIF-1	MASSIF-1
Number of frames		1500	900	1280
Oscillation step (deg)		0.1	0.2	0.1
Detector distance (mm)		393.56	234.93	302.88
Wavelength (Å)		0.9762	0.9660	0.9660
Exposure per frame (s)		0.4	0.6	0.4
Indexing and scaling				
Cell parameters	*a* (Å)	124.78	116.86	116.97
	b (Å)	191.23	191.61	190.84
	c (Å)	111.85	111.70	111.88
	α (deg)	90.00	90.00	90.00
	β (deg)	90.00	90.00	90.00
	γ (deg)	90.00	90.00	90.00
Space group		$C222_1$	$C222_1$	$C222_1$
Resolution limit (Å)		2.20	2.90	2.36
Number of total reflections		381,336	189,409	248,337
Number of unique reflections		67,838	28,263	51,562
Average multiplicity[a]		5.6 (5.4)	6.7 (6.5)	4.8 (4.8)
$<I/\sigma(I)>$		8.0 (0.8)	7.4 (1.4)	14.7 (2.0)
R_{meas}		0.167 (2.804)	0.197 (1.170)	0.077 (0.835)
Completeness (%)		99.8 (99.5)	99.9 (100)	99.7 (98.8)
Monomers per asymmetric unit		2	2	2
Solvent content (%)		59.40	61.82	61.76
B-factor (Wilson plot, $Å^2$)		35.4	35.4	35.4
Refinement				
Resolution range (Å)		50.02–2.20	29.84–2.90	29.87–2.36
Number of protein atoms		6823	6615	6693
Number of ligand atoms		2	64	56
Number of water molecules		122	98	293
R		22.74	20.10	19.9
R_{free}		26.90	23.80	22.9
Rms deviations from ideal values[b]				
Bond lengths (Å)		0.012	0.010	0.009
Bond angles (deg)		1.56	1.14	1.07
B-factor (average, $Å^2$)		58.36	61.23	54.70
MolProbity validation[c]				
Clashscore		2.33	4.20	1.48
Poor rotamers (%)		0.14	1.17	0.72
Ramachandran plot				
Favored (%)		97.25	97.07	98.26
Allowed (%)		2.75	2.93	1.74
Disallowed (%)		–	–	–

[a] Values in parentheses correspond to the highest resolution shell.
[b] Engh & Huber, 1991.
[c] Chen, 2010.

An important difference between NtrX and NtrC1/NtrC4 structures is that the last two proteins have the signature GAFTGA motif in their AAA+ domains. In *B. abortus* NtrX, this specific sequence is not presentm but the structure in this region is similar, with an insertion in a helix that forms a shorter loop and has two glycine residues (G218 and G219) that close the tip (denoted here as "MDGG loop") (Fig. 2a). Given the strict requirement for the GAFTGA conservation to interact with the σ^{54} factor, the modification in several NtrX orthologs (Fig. 2b) would preclude contacting this factor, but preserving the loop could have functional implications (see Discussion).

Several interfaces are involved in the stabilization of a dimeric structure

Analysis of NtrX crystal structure indicates an extensive interface (1900 $Å^2$) between the unphosphorylated REC domains, which includes its secondary structure elements α4-β5-α5 (Fig. 3a). This finding is in agreement with the structures of non-activated REC domains from other RRs such as NtrC1 [20], NtrC4 [21], and DctD [22], but it is in striking contrast with the reported interface for a construct of the NtrX REC domain that includes residues 1–126 but lacks the last 9 amino acids of the

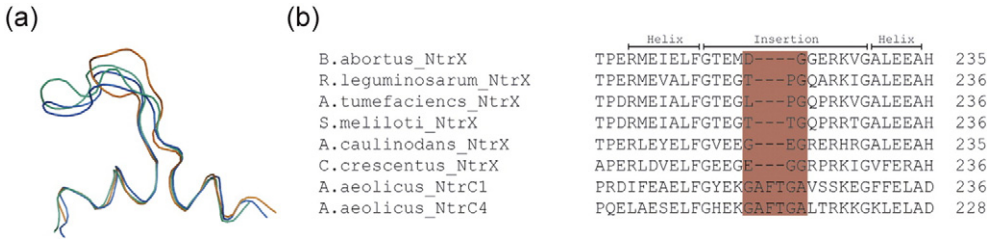

Fig. 2. (a) Structural alignment of the MDGG loop in NtrX (orange) with the GAFTGA-containing loop in NtrC1 (blue) and NtrC4 (green). (b) Multiple sequence alignment of several NtrX orthologs from *B. abortus*, *Rhizobium leguminosarum, Agrobacterium tumefaciens, Sinorhizobium meliloti, Azorhizobium caulinodans*, and *Caulobacter crescentus,* with NtrC1 and NtrC4 from *Aquifex aeolicus*. The sequences correspond to the region illustrated in panel (a), indicating above the alignment the residues that are part of the helical region and those that belong to the protruding insertion. The red box indicates the GAFTGA motif in canonical bEBPs, highlighting the deletion of residues in the different NtrX homologs.

α5 helix [15]. In this case, the BSA of the interface is dramatically reduced (to 400–600 Å^2) since only the α4-β5 elements are part of it (Fig. 3b). Given that the backbone of the REC domain in full-length NtrX superposes very well with the truncated construct (RMSD value of 0.60 Å for 119 aligned residues), eliminating the C terminus of the α5 helix leads to a rigid body movement of one of the chains (Fig. 3c) that distorts the interface. Using the PDBeFold server, a rotation–translation matrix was obtained to calculate

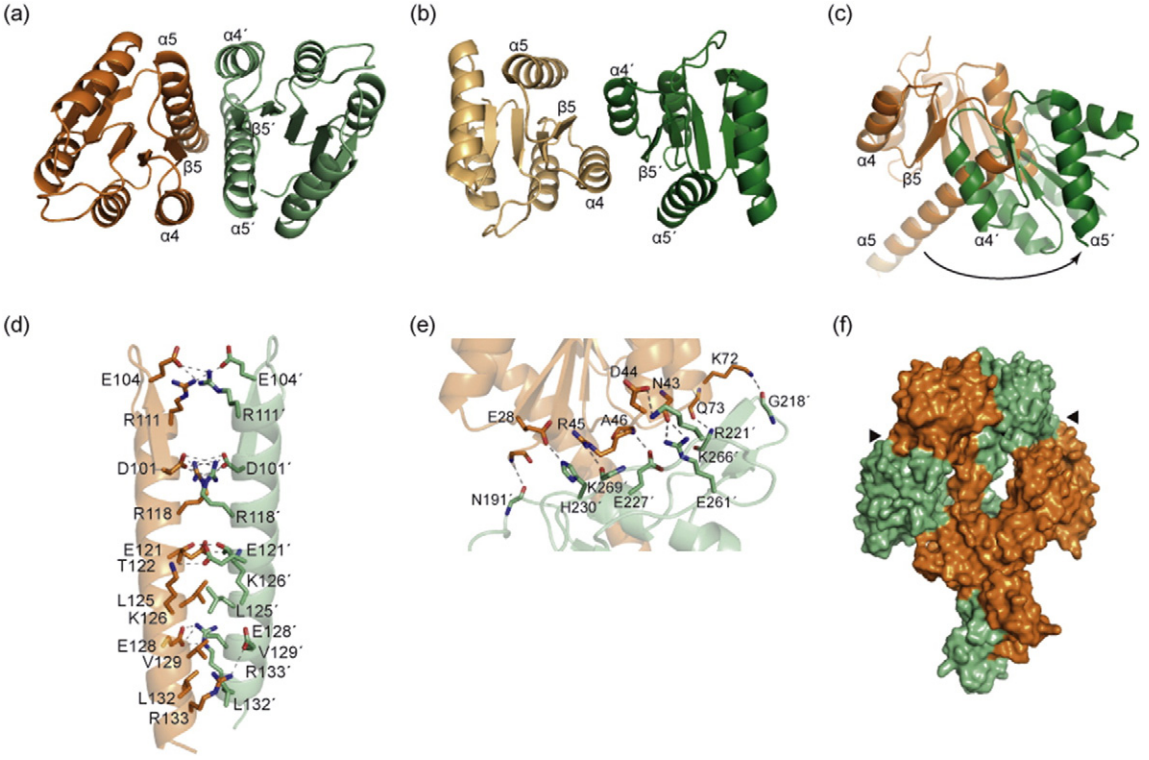

Fig. 3. Interfaces involved in the stabilization of dimeric NtrX. (a) View of the REC domains in full-length NtrX, with each chain in a different color (A, orange; B, light green) and the secondary structure elements involved in the interface indicated. (b) Truncated REC domain (PDB 4D6X, residues 1–126) with each chain in a different color (A, wheat; B, dark green) and the secondary elements involved in the interface indicated. (c) Overlay of chain B from the REC domain in full-length NtrX (orange) with the same chain from the truncated domain (green) obtained after aligning chains A (which, for clarity, are not shown). The arrow indicates the rigid-body movement caused by the different dimeric assembly. (d) Detailed interactions between the residues that participate in the REC domain interface in full-length NtrX. (e) Detailed interactions between the residues that participate in the REC-AAA interface. (f) Surface representation of NtrX indicating with triangles the interface formed between the REC and AAA+ domains from different chains.

that there is a 66° movement in chain B between the REC domain in full-length NtrX and in the truncated construct.

Several salt bridges (D101-R118′, E104-R111′, E121-K126′, E128-R133′) and hydrogen bonds (Y100-Y100′, T122-T122′) stabilize the interface between chains of the REC domains (Fig. 3d). Also, the C termini of the α5 helices cross each other and present a group of hydrophobic amino acids (L125, V129, L132) that make a pseudo coiled-coil. Despite that the analysis of the α5 helix sequence using programs that predict coiled-coils (PairCoil2, COILS) gives scores under the threshold value, it is possible to find two heptad repeats (Fig. SI5). The first one is an imperfect heptad because position *a* (in coiled-coil nomenclature) is not occupied by a hydrophobic amino acid (as is expected) but by a polar residue (T122). The second repeat has a canonical pattern, with hydrophobic residues in positions *a* and *d* (V129, L132) and charged residues in *e* and *g* (R133, R135). Notably, the charged residues in position *e* from both repeats form salt bridges with the charged amino acid in position *g'* from the previous heptad (Fig. SI5).

The analysis of a possible interface between the AAA+ domains using the PDBePISA server [23] indicates that it is not likely that these domains form a stable complex. Probably, this is due to the low number of salt bridges (K334-D241′) and hydrogen bonds (T201-A328′, R356-Q330′, N360-N360′, N360-E363′) formed between chains. However, the AAA+ domain of one monomer and the REC domain from the opposite chain establish salt bridges (E28-H230′, D44-K266′) and several hydrogen bonds (N43-R261′, Q73-R221′, K72-G218, A46-E227′, R45-K269′;Fig. 3e) that involve atoms from side chains, the backbone, or both and create an interaction surface (Fig. 3f). The residues are, in their majority, part of the α2 and α3 helices from the REC domain and of the helix with the insertion that contains the MDGG loop, this loop itself, and the loop 2, from the opposite AAA+ domain. This interface buries a considerable area (BSA of 655 $Å^2$) and has been previously reported in NtrC1 [20] and NtrC4 [21], where it was suggested that it maintains the central domain in an "off" conformation because it masks the region that is necessary for the oligomerization of NtrC1 and NtrC4 [20].

Finally, the helices that form the DBD from different chains are held together, generating an interface that buries 930 $Å^2$. This dimeric structure is stabilized by a salt bridge (R411-E415′, helix B) and several hydrogen bonds: L407-Y418′ (helix B), L405-V437′ (helices B and C, respectively), L405-Y418′, M403-Q422′ (helices A and B, respectively;Fig. SI6). Also, helix B presents hydrophobic residues that contribute to dimerization (i.e., F414) and position helix C. This dimeric ensemble that has the recognition helices exposed must be highlighted since it might allow DNA binding even in the absence of phosphorylation. In fact, there is a good superposition (RMSD of 1.2 Å for 47 residues aligned) between NtrX DBD and NtrC4 DBD crystallized in the presence of its binding sequence (PDB 4FTH; Fig. SI3c), supporting our previous hypothesis.

NtrX binds ATP but does not hydrolyze it

RRs that belong to the NtrC subfamily usually bind ATP and are able to hydrolyze it, coupling the released energy from this reaction with conformational changes that ultimately lead to transcriptional activation of σ^{54}-dependent promoters [11]. Binding of nucleotides and enzymatic activity reside in the AAA+ domain, which has specific motifs (such as Walker A and Walker B, among others) that are also present in NtrX sequence (Fig. SI1). Therefore, in order to understand how NtrX might act as a transcriptional regulator, it is of high relevance to determine whether it is able to bind ATP and hydrolyze it. To this end, we performed a photolabeling experiment [24]. NtrX was incubated with γ-^{32}P-ATP, and the mix was irradiated with UV light to promote the crosslinking of ATP and the protein. Then, an aliquot was run on SDS-PAGE gels, and the radioactivity was detected by autoradiography. As a negative control, the experiment was also performed using the truncated REC domain from NtrX. A strong band was observed in the radiography film in the lane where the NtrX sample was loaded, but no radioactivity was detected in the lane corresponding to the REC domain (Fig. 4a), indicating that NtrX is an ATP binding protein.

A limited proteolysis assay was performed in the absence and presence of ATP to evaluate possible conformational changes upon nucleotide binding and confirm the previous results. Incubation of the protein with the nucleotide produces a different proteolysis pattern, with protection of fragments of higher molecular weight (Fig. 4b), supporting that NtrX is able to bind ATP.

In order to study the binding reaction in solution, we employed fluorescence spectroscopy with a probe called Mant-ATP. The Mant group is sensitive to the chemical environment, and when it binds to a protein, it increases its fluorescent emission due to Fluorescence Resonance Energy Transfer (FRET). In a preliminary experiment, the spectra of free NtrX and Mant-ATP were obtained (setting the excitation wavelength to 290 nm), observing low emission at 448 nm (Fig. 4c). In the presence of the protein, the Mant-ATP emission peak increases significantly, an effect that can be reverted by the addition of ATP (Fig. 4c).

The fluorescent probe was also used in titration experiments to determine the affinity for ATP and ADP, using a previously described method [25]. Titration with the probe in the presence of a constant concentration of

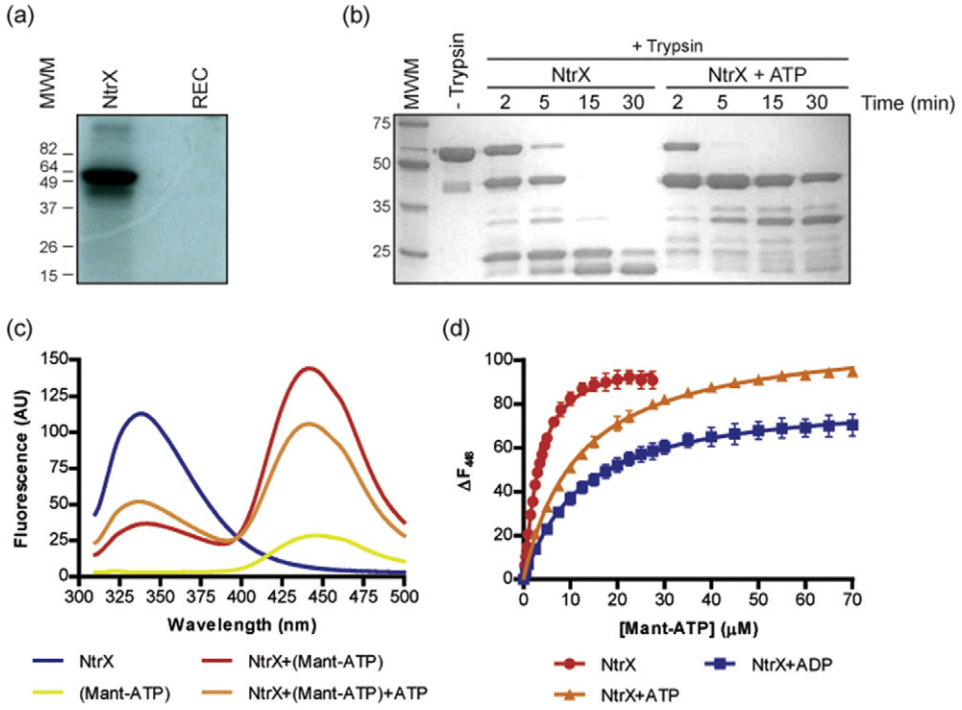

Fig. 4. NtrX is an ATP binding protein. (a) Samples of NtrX and its truncated REC domain (control) were incubated with γ-^{32}P-ATP and irradiated with UV light. Aliquots of each sample were analyzed by SDS-PAGE using a molecular weight marker (MWM) as reference. The gels were revealed by autoradiography. (b) Limited proteolysis assay. Samples of NtrX and of the protein preincubated with ATP (NtrX + ATP) were treated with trypsin. At the indicated times, aliquots were taken to be analyzed by SDS-PAGE. The gels were also loaded with a sample of the untreated protein (-trypsin) and were stained with Coomassie Blue to visualize the different bands. (c) Fluorescence spectra (λ_{exc}: 290 nm) of NtrX (5 μM), free Mant-ATP (50 μM), Mant-ATP in the presence of NtrX, and Mant-ATP with NtrX and ATP (300 μM). (d) Titration curves of NtrX (5 μM) with different concentrations of Mant-ATP in the absence of nucleotides or with constant concentrations (200 μM) of ATP or ADP. ΔF_{448} is the fluorescence intensity at 448 nm after the addition of Mant-ATP to NtrX corrected by the fluorescence of the free probe at each concentration. The curves were fitted to a specific binding model using the Hill coefficient.

ATP (Fig. 4d) gave a K_d value of 71 μM for the nucleotide, which is similar to those reported for other proteins with AAA+ domains that participate in transcriptional regulation, such as NtrC (K_d = 105 μM, [26]) and PspF ($K_{dATPγS}$ = 34 μM, [27]). Finally, the titration was performed in the presence of a constant concentration of ADP (Fig. 4d), and the binding model estimated a K_d of 70 μM. In all the cases, fitting of the curves resulted in a Hill coefficient close to 1, indicating that there is no cooperativity for binding the nucleotides.

Having established that NtrX binds ATP, we wondered if the nucleotide could be hydrolyzed. Since most of the RRs that belong to the NtrC subfamily require phosphorylation to exhibit ATPase activity [28], we verified first that NtrX can be phosphorylated *in vitro* using the small-molecule phosphodonor acetyl phosphate (AcP) [29]. The protein was incubated with AcP and Mg^{2+}; samples were taken at different times and they were analyzed in SDS-PAGE gels prepared with Phos-tag™, a tag that polymerizes with the acrylamide and decreases the migration speed of phosphorylated proteins. The results show that as time passes, there is an increase in the intensity of a low mobility band (which corresponds to phosphorylated NtrX, NtrX~P) and a decrease in the amount of protein in the unphosphorylated band (Fig. SI7a), validating the use of AcP to phosphorylate NtrX. Also, to determine if there are global conformational changes linked to NtrX phosphorylation, we performed a limited proteolysis assay. Samples of the unphosphorylated protein or NtrX preincubated with AcP were treated with trypsin, and at different times, aliquots were removed and analyzed by SDS-PAGE. The polyacrylamide gels revealed that the proteolysis pattern is different when the protein is treated with AcP (Fig. SI7b). In this case, bands of high molecular weight are more resistant to the action of the protease; meanwhile, the unphosphorylated protein is completely degraded after 20 min (Fig. SI7b). It can be concluded that treating NtrX with AcP leads to the phosphorylation of the protein and to conformational changes that alter the accessibility to the protease.

Finally, ATPase assays were performed, and neither unphosphorylated NtrX nor NtrX preincubated with AcP produced an increase in hydrolyzed ATP, indicating that this RR does not present ATPase activity (Fig. SI8). This finding is in accordance with other NtrC-like RRs that do not have a GAFTGA motif and do not hydrolyze ATP, such as *R. capsulatus* NtrC [13], and HupR [30].

Crystal structure of NtrX in complex with ATP and ADP

NtrX crystals were soaked with ATP and ADP using the CrystalDirect™ chemical diffusion technology [16], leading to the crystal structures of NtrX in complex with both nucleotides.

The crystal structure of NtrX-ATP was solved at a resolution of 2.90 Å. The initial electron density map established the presence of the nucleotide in the ATP binding pocket of the AAA+ domain, and it was clearly visible the occupancy and density of the gamma phosphate, indicating that the ATP had not been hydrolyzed. However, no electron density in the AAA+ domain could be interpreted as the Mg^{2+} ion (the Mg^{2+} was present only in the REC domain). The ATP molecule locates in a cleft between the α/β and helical subdomains of the AAA+ domain (Fig. 5a). The binding is stabilized by interactions between residues from the linker 1 (V143) and the adenine ring, from the Walker A motif (G173, A174, G175, K176, E177) and the phosphate atoms (involving mostly the backbone, but also the side chain of K176), and arginine residues that belong to the sensor 2 motif (R356 and R359) and the gamma phosphate and the ribose (Fig. 5b). Also, the side chain of R370 from the opposite monomer forms a salt bridge with the gamma phosphate.

In the presence of ATP, the overall structure of the NtrX dimer is very similar to the conformation of the apoprotein (Fig. SI9a), with an RMSD value of 2.25 Å (838 residues aligned). Individual chains of the REC domain in the free and nucleotide-bound forms align well (RMSD <0.70 Å), and the dimeric arrangement superposes with an RMSD value of 1.40 Å between both states. Inspection of this superposition indicates that there is a slight rearrangement of the interface in the structure with the nucleotide, with a 13° movement of one chain with respect to the apo state (Fig. SI9b). Despite this difference, the number of contacts involved in the interface is conserved, and the BSA is only 100 $Å^2$ smaller compared to the dimeric domain in the absence of ATP. In the AAA+ domain, there is a change in the relative position of the helical subdomain with respect to the α/β subdomain upon nucleotide binding (Fig. SI9c). Nevertheless, this does not have an impact on the number of interactions between chains or with the REC domain.

The NtrX–ADP complex structure was solved at a resolution of 2.4 Å. The interactions that participate in ADP binding are also present in the ATP complex, with only a few exceptions: in the structure with ADP, the absence of the gamma phosphate allows the R356 to form a salt bridge with oxygen atoms from the beta phosphate; besides, R356 and R359 do not interact with ribose oxygens. The overall structure of NtrX does not present important differences between each one of the nucleotide-bound forms, since superposing the complexes results in an RMSD value of 0.32 Å with 868 residues aligned.

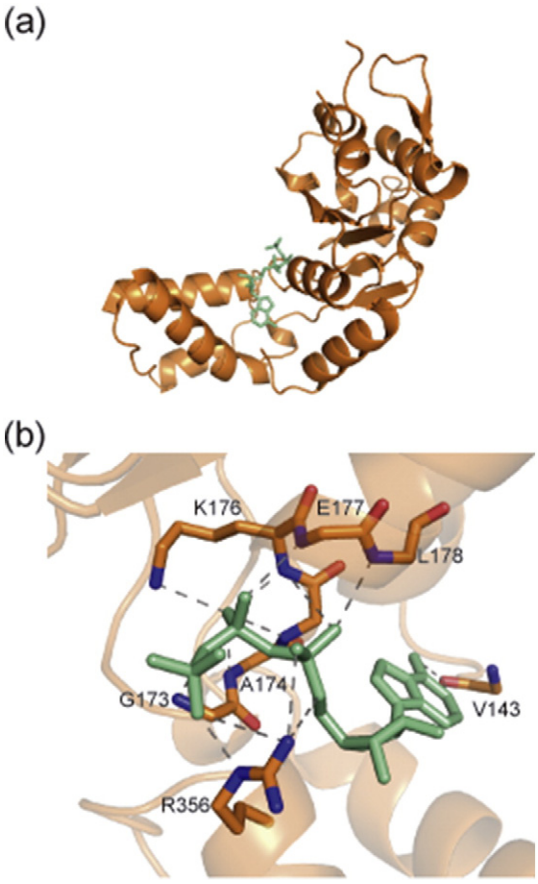

Fig. 5. ATP binding site. (a) Cartoon representation of the AAA+ domain with ATP (light green) bound to a cavity between the α/β and helical subdomains. (b) Detailed interactions between the ATP molecule (light green) and the residues in the AAA+ domain.

Through the analysis of bEBP structures with different nucleotides, some common features have been proposed to participate in the conformational transitions that couple nucleotide hydrolysis with the position of the GAFTGA loop [11,31]. One of such features is called “Asn-Glu Switch”, according to which in the ATP state, the Glu residue of the Walker B motif interacts with a conserved Asn residue; meanwhile, after hydrolysis (ADP bound), the Glu interacts with a Thr residue *via* a water molecule. In NtrX structure, it is not the Walker B Glu that interacts with the conserved Asn (N198), but the Asp residue

(D237;Fig. SI9d). In the apo state, both amino acids are 3.1 Å apart, while in the presence of ATP, they are at a distance of 2.8 Å and with ADP at 4.1 Å (Fig. SI9d). The Walker B glutamate (E238) interacts with the side chain of the conserved Thr (T278) in the absence and presence of both nucleotides (Fig. SI9d). This indicates that the conserved residues involved in the "N-E switch" present a different network of interactions in NtrX with respect to canonical bEBPs that hydrolyze nucleotides.

Also, it has been proposed that the positions of loop 1 (GAFTGA) and loop 2 of the AAA+ domain respond to the nucleotides bound by a bEBP [11,31]. The ATP-bound structures of bEBPs indicate that both loops are in a raised conformation, while after hydrolysis, the loops 1 and 2 adopt a closed conformation. In NtrX, binding of either nucleotides led to increased flexibility in the MDGG loop (loop 1) that caused weak electron density that did not allow the modeling of some residues of the loop. Nevertheless, the structure of the first residues of the insertion where it is located indicate that the tip of the loop moves with respect to the apo state, but no differences were observed between the ATP and ADP states (Fig. SI9e).

NtrX is a dimer in solution

bEBPs are typically dimeric in their inactive state and in response to a stimulatory signal the oligomerization of the bEBP is facilitated [11]. This self-association must occur in order to form the functional activator. For this reason, oligomerization of the transcriptional regulator is an important target to control its activity [11]. Therefore, we decided to determine the quaternary structure of NtrX and the influence exerted by nucleotide binding and phosphorylation using light scattering techniques.

First, a sample of unphosphorylated NtrX was injected in a size-exclusion chromatography (SEC) column and analyzed by static light scattering (SLS). The protein eluted as a single peak (Fig. 6) with a molecular mass of 104 kDa, indicating that NtrX is a dimer in solution (the molecular mass expected for a monomer would be 53 kDa). This finding is in agreement with the crystallographic dimer reported above and is consistent with the general concept of NtrC-like RRs organized as dimers in their inactive state. Another sample of NtrX was preincubated with AcP and then analyzed by SEC-SLS. In this case, NtrX also eluted as a single peak in a volume slightly increased with respect to the unphosphorylated protein (Fig. 6) and with a molecular mass of 101 kDa, suggesting that phosphorylation does not alter the quaternary structure of NtrX. The addition of ATP to the protein and the SEC buffer did not modify substantially the elution profile (Fig. 6), producing only a modest increase in the average molecular mass estimated by SLS (117 kDa). NtrX was treated

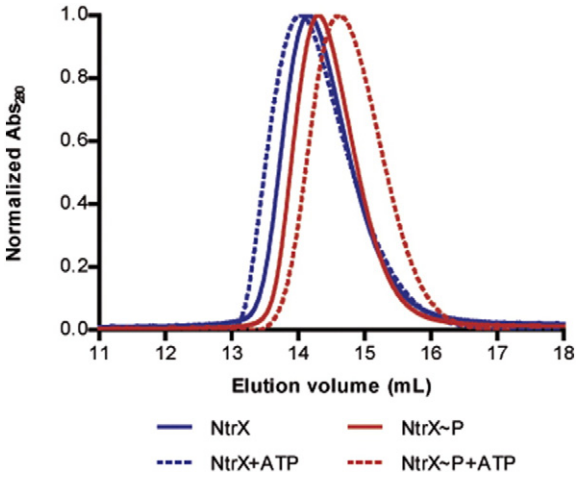

Fig. 6. SEC profiles of different samples of NtrX: unphosphorylated, bound to ATP, preincubated with AcP (NtrX~P), and preincubated with AcP in the presence of the nucleotide. The SLS signal at 90° was also recorded (data not shown) and used, along with the corresponding absorbance at 280 nm, to determine the average MM.

with AcP in the presence of ATP and eluted from the SEC column in a slightly increased volume (Fig. 6) with a molecular mass of 101 kDa, indicating that the nucleotide does not influence the oligomeric state of the phosphorylated protein. As a control, aliquots of the peaks from the samples treated with AcP were run on gels with affinity for phosphoproteins, demonstrating that at least 50% of the protein was phosphorylated (data not shown).

Since SEC is a technique that dilutes the protein sample, it is possible that a potential oligomer is formed, but it could be dissociated during the chromatography. To overcome this limitation, we measured the hydrodynamic diameter of NtrX (at different concentrations) by dynamic light scattering (DLS; Table 2). Addition of ATP to the protein produced only a slight increase in the diameter (Table 2), while preincubation with AcP and the nucleotide led to a modest decrease in comparison to the unphosphorylated apoprotein (Table 2). Neither of the treatments increased significantly the hydrodynamic diameter, as would be expected if NtrX formed an oligomer, supporting that ATP binding and phosphorylation do not alter the quaternary structure. Nevertheless,

Table 2. NtrX hydrodynamic diameter under different conditions obtained by dynamic light scattering (DLS)

[NtrX] (μM)	-ATP -AcP	+ATP -AcP	+ATP +AcP
160	7.831 ± 0.209	8.287 ± 0.115	7.571 ± 0.170
95	7.303 ± 0.279	7.364 ± 0.255	6.813 ± 0.327
48	7.059 ± 0.275	7.174 ± 0.099	6.806 ± 0.228

The results are expressed as the mean ± SD.

the hydrodynamic properties of the protein are slightly modified, in accordance with the different elution volumes in the SEC.

NtrX binds to its own promoter in a sequence that overlaps the ATG codon of the *ntrY* gene

There are only a few reports of operons whose transcription is directly regulated by NtrX. Among them, some examples are the *puf* operon from *R. capsulatus* [32] and the *putA* and *glnA* operons from *E. chaffenssis* [7]. However, there is no sequence in the *B. abortus* genome that has been reported to be a target of NtrX, and therefore, we decided to identify promoters with NtrX binding sites.

Taking as a precedent that the NtrY/X TCS regulates the expression of denitrification genes in *B. abortus* [3], we designed probes for the promoters of the nitrite reductase and the nitric oxide reductase operons. These DNA fragments were used in electrophoretic mobility shift assay (EMSA) experiments to assay the ability of NtrX to bind them, but the mobility of the probes was not modified by the protein (data not shown), indicating that NtrX does not bind directly to the nitrite reductase and nitric oxide reductase promoters.

Since many TCS are autoregulated, we decided to test the binding of NtrX to an internal promoter of its operon, which is upstream of the *ntrY* gene (Fig. SI10a). A probe for this promoter was constructed (designated pYX) and incubated with different amounts of NtrX. At concentrations higher than 0.5 μM, the protein reduced the electrophoretic mobility of the probe (Fig. 7a), indicating that unphosphorylated NtrX binds pYX. Besides, the protein concentration required to produce the probe retardation is higher than that typically reported for other RRs, suggesting that the pYX promoter contains low affinity binding sites. Also, increasing concentrations of NtrX produce complexes that migrate at different positions, but only one band is observed at each protein concentration. Such unusual DNA binding properties could be a consequence of the partial dissociation of the protein–DNA complexes during the electrophoresis [33] due to a weak interaction.

As a control, a promoter that is not expected to be recognized by NtrX (pDOQU) was incubated with the protein (Fig. 7a). The specificity of pYX recognition was further assayed by competition experiments, in which the binding reactions were performed using a fixed concentration of the protein and the pYX probe and using different amounts of a specific (unlabeled promoter) or unspecific (unlabeled pDOQU) competitor. Unlike pDOQU, the unlabeled promoter displaced the probe, increasing the proportion of free pYX (Fig. SI10b) and demonstrating that NtrX binds specifically to pYX.

Phosphorylation of *E. chaffensis* NtrX leads to higher affinity for the promoter regions of the *glnA* and *putA* operons [7]. In order to establish if phosphorylation has an effect on the affinity toward pYX, EMSA experiments were done with the radiolabeled probe and NtrX preincubated with AcP. The protein concentration at which a shift in pYX migration is observed is the same despite the preincubation with AcP (Fig. 7b), suggesting that the affinity for this DNA fragment is not modified by phosphorylation. It would be interesting to determine if binding affinity responds to protein phosphorylation in promoters with tighter interaction sites.

Having identified pYX as a target of NtrX, we wanted to establish the nucleotide sequence that is recognized by the RR and to determine if the phosphorylation alters the binding site within the promoter. For this, DNAse I footprinting assays were performed with unphosphorylated NtrX and the protein preincubated with AcP. Preliminary experiments were conducted to define the best probe to be used, which was finally designed with 100 nt upstream of the *ntrY* initiator ATG and 70 nt downstream of this site (Fig. SI10a). This probe exhibited different digestion patterns in the presence of NtrX, with protected and hypersensitive sites (Fig. 7c). Sequencing of these regions allowed us to determine the binding site, which is approximately 50 bp long and presents a palindromic sequenceand an upstream hemisite (Fig. 7d). Analysis of the digestion pattern suggests that unphosphorylated NtrX binds to the hemisite; meanwhile, the protein preincubated with AcP binds to the hemisite and the palindromic sequence (Fig. 7c and d). It is important to highlight that the sequence recognized by NtrX overlaps the ATG initiator codon of the *ntrY* gene, and it includes a part of its coding sequence.

NtrX represses transcription from the pYX promoter

As has been mentioned, an important feature of the NtrX binding site is that it overlaps with the coding sequence of the *ntrY* gene. This could indicate that the binding of the RR is an obstacle to the advance of the RNA polymerase during transcription, establishing a mechanism to repress its own expression. To test this hypothesis regarding the regulatory role of NtrX, we performed an *in vivo* reporter assay. For this, two plasmids were constructed: a reporter plasmid with the *lacZ* gene cloned under the control of the pYX promoter, and an expression plasmid in which full-length NtrX was introduced under the control of the promoter of the T7 RNA polymerase. As controls, an expression plasmid with the truncated REC domain of NtrX and a plasmid with no construct were used. Then, the reporter plasmid was cotransformed with each of the expression plasmids in *Escherichia coli* BL21 pLys. We chose this organism because it was not possible to obtain a *B. abortus* strain with the *ntrX* gene deleted, and *E. coli* does not

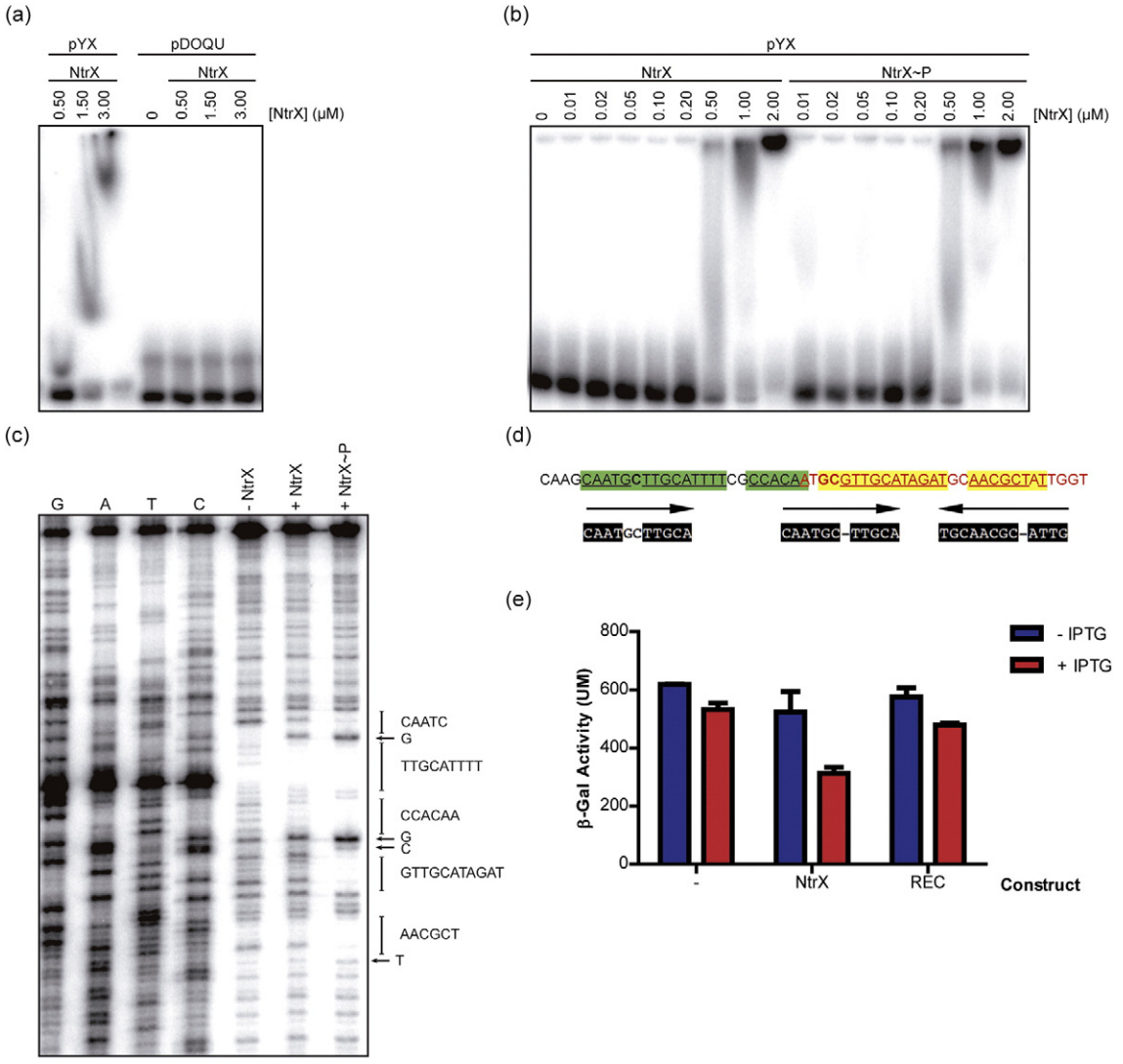

Fig. 7. DNA binding experiments and transcriptional activity of NtrX. (a) EMSA performed with different concentrations of NtrX (indicated) and the probes pYX and pDOQU (control). (b) EMSA with increasing amounts of unphosphorylated NtrX or NtrX preincubated with AcP (NtrX ~ P) and the radioactive promoter pYX. (c) Footprinting assay to determine the binding site of pYX. The probe was digested with DNAse I in the absence of NtrX (-NtrX) or after the addition of either the unphosphorylated RR (4 μM) or NtrX preincubated with AcP (NtrX ~ P). Sequencing reactions were carried out and loaded in the same gel (G, A, T, C). Protected regions are indicated to the right of the gel with a vertical line; meanwhile, hypersensitivity sites are indicated with an arrow. The sequence corresponding to each section is written to the right. (d) Fragment of the pYX probe with the coding sequence of the *ntrY* gene in red letters and non-coding nucleotides in black. Underlined letters correspond to the protected regions obtained in the footprinting assay, while the bold nucleotides are the hypersensitive sites. Green boxes indicate the identified binding sites for unphosphorylated and phosphorylated NtrX, while the yellow boxes highlight those sites bound by the RR preincubated with AcP. Analysis of this fragment shows the presence of a palindromic sequence (opposite arrows on top) and an upstream hemisite. (e) *In vivo* reporter assay. The β-galactosidase activity (expressed in Miller Units) of different strains of *Escherichia coli* BL21 pLys was measured in uninduced cultures (blue bars) or after the addition of IPTG (red bars). Each strain contained a reporter plasmid, in which the *lacZ* gene was cloned downstream of pYX, and an expression plasmid that had a T7 promoter directing the transcription of a particular construct (indicated) or that had an empty polylinker (-).

code for NtrX, avoiding possible interference from an endogenous gene.

The cotransformed strains were grown, and the β-galactosidase activity was measured in cultures that had not been induced and others that were incubated with IPTG. The high activity observed in cultures of all the strains in the absence of IPTG demonstrates that the pYX promoter is active in *E. coli* and that in the absence of the inducing agent, all the strains express comparable levels of

the enzyme (Fig. 7e). Addition of IPTG causes a slight decrease in the β-galactosidase activity in the strain transformed with the expression plasmid that does not contain a construct, reaching 86% of the activity in the presence of the inducing agent compared with the uninduced culture (Fig. 7e). However, this reduction was more dramatic when the bacteria were cotransformed with the expression plasmid containing NtrX (60%; Fig. 7e). In the strains transformed with the REC domain, the decrease in the activity levels upon induction was similar to that observed in the strain with no construct (Fig. 7d), demonstrating that the repression observed with NtrX is not caused by the overexpression of a recombinant protein *per se*.

Then, it can be concluded that the induction of the cultures with IPTG leads to the expression of NtrX, which binds to pYX and produces a significative decrease in the expression of the β-galactosidase enzyme. Therefore, NtrX acts as a repressor of the transcription from the pYX promoter.

Discussion

In this article, we report the first crystal structure of full-length NtrX, a member of the NtrC subfamily of RRs, which is also the first structure in this subfamily where the relative organization of the DBD is revealed in a full-length protein. Strikingly, despite being an atypical member of the NtrC subfamily, NtrX has a general organization that resembles those of NtrC1 and NtrC4 in their unphosphorylated states, with interfaces between the REC domains and the REC-AAA domains from opposite chains. NtrX REC domains form an interface that involves the α4-β5-α5 elements, as described in DctD [22], NtrC1 [20], and NtrC4 [21]. Also, the first two and NtrX have a long extension of the α5 helix that presents a pseudo coiled-coil that participates in the dimerization surface. Such interface is different from the dimerization surface described for a truncated construct of the isolated NtrX REC domain. In this case, the protein encompasses residues 1–126 and the interface is formed by the α4-β5 elements [15]. It is interesting to note that not only the secondary structure elements of the interface changed upon truncation of the REC domain but also the nature of the surface, since in full-length NtrX, numerous polar residues are involved, while the isolated REC domain presents an interface that is mostly hydrophobic [15]. The difference between the interface of the truncated construct and the full-length protein might reside in the absence of the last residues of the α5 helix, a hypothesis that is supported by evidence reported on the activation of DctD and NtrC1. Studies performed with these RRs have proved that mutations that weaken the α4-β5-α5 dimer (characteristic of the inactive and unphosphorylated state) lead to a partially active RR, and it has been postulated that the isolated and activated REC domains from those RRs form an α4-β5 dimer [22,34,35]. In NtrX, the truncation of the REC domain eliminated several stabilizing forces of the α4-β5-α5 dimer, particularly two salt bridges (E121-K126′ and E128-R133′) and the hydrophobic patch of the pseudo coiled-coil. Therefore, comparing NtrX with DctD and NtrC1 leads us to postulate that the C-terminal extension of the α5 helix acts as a structural "Velcro" that holds an α4-β5-α5 dimer that can be disrupted by truncating the REC domain in those residues that form the pseudo coiled-coil.

The previous analogy among DctD, NtrC1, and NtrX might also suggest that all of them share a similar activation pathway. However, the current model to understand DctD and NtrC1 activation postulates that the phosphorylation of the REC domains changes the dimerization surface (from α4-β5-α5 to α4-β5, as has been mentioned) and allows the AAA+ domains to relocate in order to form a hexamer. Several experiments were conducted here to evaluate the potential oligomerization of NtrX, and our results indicate that this protein is a dimer in solution that does not undergo further oligomerization. Given that conserved determinants responsible for promoting the oligomerization of bEBPs have not been identified yet, it is hard to explain the reasons for this difference. Nevertheless, the structure of NtrX revealed a surface of interaction between the REC and AAA+ domains, similar to that found in other NtrC-like RRs. Therefore, it is possible that upon activation, NtrX undergoes the same changes as DctD or NtrC1 in the REC domain interface, but instead of coupling them to an oligomerization process, they are transduced to the AAA+ domain, allowing the movement of motifs that could participate in different protein–protein interactions. Such interactions could involve accessory proteins, since there are many cases of RRs that utilize them to mediate signal integration, scaffolding, allosteric regulation, etc. [36]. One candidate to participate in those interactions might be the MDGG loop. Despite the lack of the GAFTGA motif, the loop where it should be located is present in NtrX, and it interacts with residues in the REC domain, raising the possibility of a functional role.

Another feature that NtrX has in common with canonical bEBPs is that it binds ATP. Some characteristic differences have been observed in a bEBP called PspF among the apo, ATP, and ADP-bound states obtained by soaking nucleotides into crystals [31]. Specific positions for a conserved asparagine and a conserved glutamate have been reported (postulating the existence of an "Asn-Glu switch") and also the movements of the GAFTGA-containing loop and the motif called loop 2. It has been proposed that these elements communicate changes in the nucleotide binding pocket to the GAFTGA motif in order to allow differential interactions with the

σ^{54} factor. In NtrX, the corresponding Asn and Glu residues (N198 and E238) arrange in a different fashion, and their position is the same in the ATP- and ADP-bound forms. Also, the MDGG loop and loop 2 do not change between both states. Since NtrX does not have a GAFTGA motif, it is possible that such conformational changes are not needed and there is no coupling between them and the nucleotide binding pocket.

Unlike classical bEBPs, NtrX does not hydrolyze ATP. This finding has also been reported for other RRs that lack a conserved GAFTGA, such as *R. capsulatus* NtrC and HupR. In the latter case, the binding of ATP has not been investigated, and the absence of activity was attributed to Walker A and B motifs that do not conserve critical residues [37]. In the case of *R. capsulatus* NtrC, binding of ATP was proved and it was demonstrated that it is necessary to activate transcription at σ^{70} regulated genes [13]. Therefore, even though NtrX does not have ATPase activity, the binding of nucleotides might have an important role in its mechanism of action.

It is broadly accepted that AAA+ ATPases usually function as higher-order oligomers and that oligomerization allows the formation of the catalytic active site at the interface between adjacent subunits of the oligomer [38]. Therefore, controlling the oligomerization of the bEBPs is a common strategy employed to regulate their ATPase activity [11]. In this context, we speculate that the absence of ATPase activity in NtrX is a consequence of the inability of the protein to form an oligomer, even in the phosphorylated state and in the presence of ATP. In this regard, the quaternary structure of *R. capsulatus* NtrC has not been determined yet, but taking into consideration our results, it would be interesting to establish whether this atypical bEBP (that does not hydrolyze ATP) forms oligomers in solution.

Other feature that has been highlighted in NtrX structure is that the DBD forms a dimer and that the DNA recognition helices in the DBD are exposed, suggesting that the unphosphorylated RR is able to bind DNA. This was confirmed by gel-shift experiments that also allowed us to identify an internal promoter of the operon that codes for NtrX (pYX) as a target sequence. Binding of unphosphorylated NtrX to the DNA was also observed in the ortholog from *E. chaffeensis*, particularly with the *putA* and *glnA* promoters [7]. However, in this case, the phosphorylation of the RR increased the affinity toward DNA [7], a result that could not be reproduced using *B. abortus* NtrX and the pYX promoter. On the contrary, differences were obtained here in the footprinting experiments performed with unphosphorylated and phosphorylated NtrX. It is difficult to speculate on a possible communicational pathway between the REC domain and the DBD because the crystal structure of NtrX did not show an extensive interdomain interface that involved the DBD and could enable the transmission of conformational changes. In fact, it has been suggested that the linker that connects the DBD with the rest of the protein might act as a flexible tether [39]. Our structure shows few contacts that stabilize the linker and lead to an asymmetric position of the DBD with respect to the remaining domains. This configuration could have some role in the interaction with the DNA since it has been recently described that asymmetry plays an important role in stabilizing the complex between the RR KdpE and its binding site in the DNA [40]. Nevertheless, it is also probable that the contacts of the linker arose as a consequence of the crystal packing, and their functional relevance should be tested *in vivo*.

In light of the previous discussion, some hypothesis can be proposed to interpret the pattern obtained in the footprinting experiment with the phosphorylated protein. In the first place, it is possible that upon phosphorylation, NtrX binds to pYX with higher cooperativity but with the same affinity toward the promoter. In this case, phosphorylation of the REC domain could be transduced into conformational changes at the AAA+ domain (a different position in the MDGG loop, for example) that facilitate interactions with another NtrX dimer that is recruited in the context of the DNA binding site, but such interactions are not strong enough to facilitate the oligomerization of the protein in solution. It has been reported that the binding at neighboring DNA sites occurs with positive cooperativity for NtrC in the unactivated state and that the cooperativity constant increases dramatically upon phosphorylation [41]. Similar propositions have been postulated for DctD on the basis of the increase in the cooperative binding detected using a truncated and constitutively active protein [42].

Other explanation for the results obtained in the footprinting assay could be that phosphorylation changes NtrX conformation in a way that a part of the protein "covers" the probe, altering the accessibility of DNAse I to the cleavage sites. This hypothesis would also sustain that the linker that connects the DBD is not merely a tether and has defined configurations and that the asymmetry in the location of this domain is regulated, playing a role in the interaction with the DNA or other accessory proteins. On the other hand, it cannot be ruled out that phosphorylated NtrX binds to its target sequence in a fashion that changes the DNA topology altering the pattern in the footprinting experiment.

Through DNA binding assays, we showed that NtrX recognizes a sequence that overlaps the first ATG codon of the *ntrY* gene, suggesting that protein binding might become an obstacle to the RNA polymerase. This notion was supported by an *in vivo* assay that showed that NtrX overexpression led to a repression of the transcription from the pYX promoter. Similar results were reported studying *R. capsulatus* NtrX and the *puf* promoter, since the RR binds to a

50-bp-long region that overlaps the translation initiation codon, and it was also demonstrated that NtrX regulates negatively this transcriptional unit [32]. This could indicate that the mechanism of transcriptional repression proposed for pYX by hindrance to the RNA polymerase advance might be extended to other operons negatively regulated by NtrX, independently of which sigma factor is necessary for its expression.

Many transcriptional regulators can act as activators and repressors depending on the nature and location of their binding sites in their target genes [43,44]. For example, in addition to being a bEBP, NtrC can repress transcription in different bacteria [45–47]. Another example is the TyrR protein, an unusual bEBP that lacks a GAFTGA motif, which can be a repressor or an activator at σ^{70} promoters [48]. Therefore, although we have presented *B. abortus* NtrX as a transcriptional repressor, it could act as an activator at other promoters. In fact, *E. chaffeensis* NtrX has been associated with the induction of genes involved in amino acids metabolism [7]. This raises questions on whether transcriptional activation is also performed by *B. abortus* NtrX and if it could be achieved through the same mechanism as canonical bEBPs. Finding answers to these matters will require the discovery of other targets bound and activated by this RR and will require to determine which sigma factor regulates their transcription. At first glimpse, NtrX conserves important motifs in its AAA+ domain, and the overall structure of the full-length protein resembles those of the classic members of the NtrC subfamily of RRs. However, NtrX does not have the structural signature motif GAFTGA, and our results indicate that the protein neither forms an oligomer in solution nor has ATPase activity. Also, the structure of NtrX in complex with nucleotides showed that conserved residues do not relocate upon nucleotide binding, as it occurs in typical bEBPs to communicate conformational changes from the nucleotide binding site. Altogether, these results would point toward a potential mechanism of transcriptional activation that might be different from the one proposed for bEBPs. Another reason that sustains this idea is that *E. chaffeensis* encodes only two sigma factors (σ^{32} and σ^{70}) [49] and three TCSs (PleC-PleD, CckA-CtrA, and NtrY-NtrX) [6]. It seems likely that given the absence of a functional σ^{54}, *E. chaffeensis* has preserved only transduction pathways that do not depend on this sigma factor to promote transcription, and it would be reasonable to presume that the mechanism of action of different NtrX orthologs is conserved.

In summary, we have provided the first crystal structure of NtrX, which indicates that the architecture of the REC and AAA+ domains is similar to other members of the NtrC subfamily of RRs that act as bEBPs. However, the biochemical data indicate that NtrX can act as a transcriptional repressor and that it does not perform several fundamental actions required to activate transcription at σ^{54} promoters. This suggests that phosphorylation of the REC domain is coupled to conformational changes at the AAA+ domain that are different from those proposed for bEBPs and point toward a different mechanism of signal transduction. Further efforts will be needed to establish whether *B. abortus* NtrX is also a transcriptional activator, to identify induced targets and the corresponding sigma factor that directs their transcription, in order to provide a complete model for NtrX-dependent transcriptional regulation.

Materials and Methods

DNA manipulations

DNA encoding full-length NtrX was amplified by PCR from *B. abortus* 2308 genomic DNA using the primers 5′-ATATGGAAAACCTGTATTTTCAGGGC ATGGCGGCCGATATTCTTGTTGTTGATGAC-3′ (which added a Tobacco Etch Protease (TEV) cleavage site upstream of the protein coding sequence) and 5′-GCCGGATCTCA GTGGTGGTGGTGGTGGTGCCTCGAGTT ATACGCCGAGAGACTTCAGCTT-3′. The resulting PCR product was used as a template in a second PCR reaction with primers 5′-AGCAGCGGCCTGG TGCCGCGCGGCAGCCATATGGAAAACCTG-TATTTTCAGGGC-3′ and 5′-GCCGGATCTCAGTG GTGGTGGTGGTGGTGCCTCGAGTTATACGCC-GAGAGACTTCAGCTT-3′. Finally, this product was inserted into the pET28 vector (Novagen) by the restriction-free cloning method [50], using it as a megaprimer in a PCR reaction with pET28 as template, followed by digestion with the enzyme DpnI. The final pET28-NtrX plasmid, the quality of which was checked by DNA sequencing, includes a 6-residue-long N-terminal His-tag separated from NtrX coding sequence (453 residues) by a TEV protease cleavage site.

The plasmids encoding NtrX with a C-terminal His-tag in the pET24 vector and the truncated REC domain (residues 1–126) were prepared as described before [3,15].

Protein overexpression and purification

BL21(DE3)pLys cells were transformed with pET28-NtrX and grown at 37 °C in 3 l of LB media with the appropriate antibiotic until absorbance (at 600 nm) reached 0.6. At this point, IPTG was added to a final concentration of 1 mM, and the culture was incubated for another 4 h at 28 °C with agitation. The bacteria were centrifuged at 7000 rpm for 10 min at 4 °C. Pellets were resuspended in lysis buffer [20 mM Tris–HCl, 200 mM NaCl, 30 mM imidazole,

and 1 mM PMSF (pH 8)], sonicated, and then centrifuged at 45000 rpm in a Beckman Coulter L7-65 ultracentrifuge for 45 min at 4 °C. The supernatant was incubated with 1 ml of nickel nitrilotriacetic acid-agarose resin (Qiagen) during 1 h with agitation in a cold room. Then, the mixture of the supernatant and resin was loaded in a plastic column (Bio-Rad) and washed twice with 25 ml of washing buffer [20 mM Tris–HCl, 200 mM NaCl, and 30 mM imidazole (pH 8)]. The protein was eluted with elution buffer [20 mM Tris–HCl, 200 mM NaCl, and 500 mM imidazole (pH 8)], and different 1-ml fractions were collected. They were analyzed by SDS-PAGE and Coomassie Blue staining to determine the samples with the highest amount of recombinant protein. The pooled fractions were mixed with TEV protease in a protein:protease ratio of 1:70 and dialyzed against buffer [20 mM Tris–HCl, 100 mM NaCl, 30 mM imidazole, and 1 mM PMSF (pH 8)] at 4 °C overnight. After that, the dialyzed protein was incubated with nickel nitrilotriacetic acid-agarose resin at 4 °C with agitation for 1 h. Then, the mix was loaded in a plastic column, and the flow-through (containing the protein without tag) was collected and further purified by gel-filtration chromatography on a Superdex 200 column (GE Healthcare) with isocratic elution in buffer [20 mM Tris–HCl, and 100 mM NaCl (pH 8)], yielding a major peak at around 79 ml, which was collected in different fractions. Samples of each fraction were analyzed by SDS-PAGE, and those with the highest purity were pooled and concentrated by centrifugation in Amicon Ultra-4 devices (Millipore) and stored at −70 °C. The protein concentration was calculated from the measured absorbance at 280 nm and the extinction coefficient obtained from the ProtParam tool [51]. All the informed concentrations refer to the protein as a monomer.

The REC truncated domain was expressed and purified as reported previously [15].

Crystallization

Crystallization trials were performed at the High Throughput Crystallization Laboratory of the EMBL Grenoble Outstation[‡], using the sitting-drop vapor diffusion method [52]. Drops of 100-nl sample and 100-nl crystallization solution were set up in CrystalDirect™ plates (MiTeGen, Ithaca, USA) using a Cartesian PixSys robot (Cartesian Technologies, Irvine, USA). The experiments were incubated at 20 °C in a RockImager system (Formulatrix Inc., Bedford, USA). Initially, NtrX crystallized at a concentration of 10 mg/ml in 4 M sodium formate using Classics Suite Screen (Qiagen, Hilden, Germany). After a round of refinement, better crystals were obtained with 3.36 M sodium formate in the crystallization reservoir.

Automated high-throughput crystal cryo-cooling and harvesting was performed with the CrystalDirectTM Technology as described elsewhere [16,53], and crystals were stored in liquid nitrogen for data collection. For the derivative crystals, lantanide compounds (Lanthanide Phasing Kit, Jena Bioscience, Jena, Germany) were soaked using the CrystalDirect technology for chemical delivery through diffusion, by adding 50-nl phasing agent to a 200-nl crystallization drop and incubating for 30 min.

For the crystals with nucleotides, solutions of ATP or ADP (35 mM) and $MgCl_2$ (35 mM) were soaked using the CrystalDirect technology, by adding 50 nl of the nucleotide solution to a 200-nl crystallization drop with grown crystals and incubating for 20 min. After the incubation, the crystals were harvested and cryopreserved as already mentioned. Follow-up and management of crystallization, crystal harvesting, and data collection experiments were done through the Crystallization Information Management System (CRIMS[§]).

Diffraction data were collected at the European Synchrotron Radiation Facility (ESRF Grenoble, France) either at ID29 [54] or at the fully automated MASSIF-1 beamline [55].

Structure determination

Crystallographic data reduction and scaling were performed with the XDS software [56]. An initial dataset at 2.8-Å resolution from an ytterbium-soaked NtrX-apo crystal was used for initial phasing and model building using SHELX [57,58] and automated chain tracing with Buccaneer. This partial model was used as a search model for molecular replacement with a 2.2-Å resolution native dataset with Phaser [59]. Successive rounds of automatic refinement and manual building were carried out with BUSTER [60] and COOT [61]. R_{free} values [62] were computed from 5% randomly chosen reflections, which were not used in the refinement. The structure was validated using Molprobity [63]. Details of data collection, processing, and structure refinement are provided in Table 1. The interface areas were obtained with PDBePISA [23], and the superpositions and RMSD calculations were performed with PDBeFold [19]. Sequence alignments were performed with Clustal Omega [64]. All figures describing the structures were prepared using the program PyMOL[‖].

The structures of NtrX with ATP and ADP were solved by molecular replacement using the NtrX apo structure as model. Detailed statistics on the refinement process are presented in Table 1.

Photolabeling with γ-^{32}P-ATP

NtrX was diluted in buffer [50 mM Tris–Ac, 5.4 mM $MgCl_2$, 1 mM DTT, and 1 mM EDTA (pH 8)] to a final concentration of 3 μM, and 2 μl of γ-^{32}P-ATP (3.66 μCi) was added. The sample was kept in

ice and irradiated with UV light produced by a UV chamber (Bio-Rad) GS Gene Linker™ for 15 min. This procedure was repeated with the truncated REC domain as a negative control.

After irradiation, the samples were mixed with Laemmli buffer, and a volume equivalent to 3 μg of protein was loaded in SDS-PAGE gels. After electrophoresis, the gel was dried and revealed by autoradiography.

Equilibrium fluorescence spectroscopy with Mant-ATP

All fluorescence measurements were made using a Jasco FP-6500 spectrofluorimeter. Sample temperature was held at 25 °C by a circulating water bath.

Binding of Mant-ATP (Molecular Probes) was monitored, preparing 500-μl samples containing 50-μM probe in binding buffer [50 mM Tris-Ac, 200 mM NaCl, 5.4 mM $MgCl_2$, 1 mM DTT, and 0.1 mM EDTA (pH 8)]. Emission spectra between 310 nm and 500 nm were then acquired by exciting the samples at 290 nm (excitation and emission slits were set to 3 nm). NtrX was next added directly to the cuvette to a final concentration of 5 μM, and the fluorescence spectra were reacquired. Finally, 320 mM ATP was added to monitor the Mant nucleotide displacement from the active site. Control experiments were carried out in the absence of NtrX to ensure that ATP did not alter the fluorescence emission of the Mant nucleotide.

Nucleotide affinities obtained by fluorescence spectroscopy

The general protocol used has been described elsewhere [25]. Briefly, titrations of Mant-ATP were carried out in binding buffer [50 mM Tris-Ac, 200 mM NaCl, 5.4 mM $MgCl_2$, 1 mM DTT, and 0.1 mM EDTA (pH 8)] and 5 μM NtrX. Microliter quantities of Mant-ATP were added to 500-μl samples from stock solutions of fluorescent nucleotide. Changes in fluorescence intensity were monitored by obtaining emission spectra between 310 nm and 500 nm by excitation at 290 nm (excitation and emission slits were set to 3 nm) as a function of increasing Mant nucleotide concentration. A background sample titration lacking NtrX was carried out for each titration of Mant nucleotide in the presence of the protein. For the measurement of dissociation constants for ADP and ATP, titrations were performed as described previously in the presence of the competing nucleotide at a concentration of 200 μM. Each curve was performed in duplicate.

The observed fluorescence intensity at any given concentration of Mant-ATP in the presence of the protein was corrected by the corresponding value in the curve of the free nucleotide ($\Delta F = F_{\text{Mant+NtrX}} - F_{\text{Mant}}$) at 448 nm (emission maximum), and the change in fluorescence was plotted against the concentration of the probe. Data were adjusted to a specific binding model using the Hill coefficient (GraphPad Prism) to obtain the K_d for Mant-ATP (K_d^{Mant}).

For titrations in the presence of fixed amounts of competing nucleotides, data analysis was performed as already published [25]. The plots yield apparent K_d values for Mant-ATP ($^{\text{app}}K_d^{\text{Mant}}$). The true K_d values for the competing ligands were calculated using equation:

$$K\text{d}_{\text{app}}^{\text{Mant}} = K\text{d}^{\text{Mant}}\left(1 + \frac{[\text{L}]}{K\text{d}^{\text{L}}}\right)$$

where [L] and K_{dL} are the concentration and dissociation constants for the competing nucleotide.

In vitro phosphorylation with AcP

Phosphorylated NtrX was generated by incubation of the protein (at the concentration needed in each assay) with 30 mM AcP and 30 mM $MgCl_2$. This reaction was carried out at room temperature during 1 h, and then, the protein was centrifuged at 14000 rpm for 10 min prior to its use.

ATPase assay

The ATPase activity was determined using the ADP-Glo™ Kinase Assay (Promega) according to the manufacturer's recommendations. This assay measures the ADP formed from a kinase or ATPase reaction and therefore avoids the interference of compounds with labile phosphates (such as AcP). The experiment was performed at 25 °C (room temperature) in a reaction buffer [20 mM Hepes, 150 mM NaCl, 2 mM DTT, 4 mM $MgCl_2$, and 5% glycerol (pH 7.5)] with different concentrations of NtrX (unphosphorylated or preincubated with AcP) and a final ATP concentration of 0.25 mM. After 30 min, the reaction was quenched and the luminescent signal was measured. A calibration curve with known concentrations of ADP was used to transform the luminescent signal into the concentration of hydrolyzed ATP. The experiments with NtrX were performed in triplicate, and the protein *ch*LGP2 (incubated with an activator 12 dsRNA) was used as a positive control.

Phosphoprotein affinity gel electrophoresis

Phos-tag™ acrylamide running gels contained 15% (wt/vol) 29:1 acrylamide/*N*′*N*′-methylenebisacrylamide, 375 mM Tris (pH 8.8), and 0.1% (wt/vol) SDS. Gels were copolymerized with 75 μM Phos-tag™ and 150 μM $ZnCl_2$. Stacking gels contained 4% (wt/vol) 29:1 acrylamide/*N*′*N*′-methylenebisacrylamide, 125 mM Tris (pH 6.8), and 0.1% (wt/vol) SDS. All

Phos-tag™ acrylamide containing gels were run with standard denaturing running buffer at 4 °C under constant voltage (150 V). The gels were stained with Coomassie Blue to visualize the protein bands.

Limited proteolysis to evaluate *in vitro* phosphorylation

To test the global effects of ATP binding on NtrX conformation, two aliquots were diluted in reaction buffer (50 mM Tris-Ac, 5.4 mM $MgCl_2$, 1 mM DTT, 1 mM EDTA, and 10% glycerol) to a final concentration of 8 μM. ATP (1 mM) was added to one of them and it was incubated at room temperature for 20 min. After this time, trypsin was added to both samples in a protein:protease ratio of 1:25. The reaction was performed at room temperature, and at different times, aliquots were removed and the proteolysis was quenched by the addition of Laemmli buffer. The aliquots were heated and a volume equivalent to 10 μg of NtrX was loaded in SDS-PAGE gels that were finally stained with Coomassie Blue.

To evaluate the *in vitro* phosphorylation of NtrX, two dilutions (10 μM) were prepared in buffer [20 mM Tris–HCl, and 200 mM NaCl (pH 8)]. One of them was incubated with 30 mM AcP and 30 mM $MgCl_2$ for 80 min at room temperature. After that, glycerol (at a final concentration of 5%) and trypsin (ratio protease:protein 1:20) were added to both samples. The digestion preceded at 25 °C, and at different times, aliquots were taken and the reaction was quenched by the addition of SDS-PAGE loading buffer. The rest of the assay was carried out as mentioned previously.

SLS

The average molecular mass of NtrX was determined by SLS using a Precision detector PD2080 light scattering instrument connected in tandem to a high-performance liquid chromatography system and an LKB 2142 differential refractometer. In each case, 500 μl of protein solution (at a concentration of 100 μM) was injected into an analytical Superdex 200 column and eluted with a buffer consisting of 20 mM Tris–HCl and 200 mM NaCl (pH 8). The 90° light scattering, absorbance at 280 nm, and refractive index signals of the eluted protein were analyzed with the Discovery32 software supplied by Precision detectors. The 90° light scattering detector was calibrated using bovine serum albumin (MM: 66.5 kDa) as a standard.

For samples containing ATP, the nucleotide and $MgCl_2$ were added to the protein and the elution buffer at a concentration of 4 mM.

DLS

NtrX hydrodynamic diameter was determined by DLS using a Zeta Sizer NanoS instrument (Malvern) at 20 °C using a 3-mm quartz cuvette (sample volume: 30 μl). A stock solution of the protein was used to prepare different dilutions (160 μM, 95 μM, 48 μM) in a buffer [20 mM Tris–HCl and 200 mM NaCl (pH 8)] previously filtrated using a 0.22-μm filter. All samples were centrifuged (14,000 rpm, 10 min) at 4 °C before the measurements. The informed values correspond to an average of six measures and its standard deviation.

To investigate the effect of ATP, we added the nucleotide and $MgCl_2$ to the diluted protein at a final concentration of 4 mM.

EMSA

Probes were internally labeled by PCR through the inclusion of 40 mCi of [α-^{32}P]-dCTP in the reaction mixture and were subsequently purified on native polyacrylamide gels. Probe pYX and a control probe were generated by PCR using Taq polymerase, genomic DNA of *B. abortus* S2308 as template, and primers 5′-CCGCGGCAACCAGATCAAGG-3′ and 5′-TAATACCCGGTAAGGCGAGA-3′ (for amplifying pYX), or 5′-CTATGCAACCCAGAAGGTCGG-3′ and 5′- GGGAATTCGTCAGGCACAATAAAGTCAC-3′ (for obtaining the control pDOQU). The EMSAs were performed in a volume of 20 μl containing DNA-binding buffer [10 mM Tris-Ac, 100 mM KAc, 8 mM $MgAc_2$, 35 mM NH_4Ac, 0.5 mM DTT, 2 mM ATP, 3% glycerol, 10 μg ml^{-1} BSA, and 1 mg DNA salmon sperm (pH 8)], 10,000 cpm of the ^{32}P-labeled probe, and NtrX recombinant protein. After incubation at room temperature for 30 min, the protein–DNA complexes were separated from the free probes by electrophoresis in 8% non-denaturing polyacrylamide gels at a constant voltage of 220 V. The gels were dried and exposed to a Storage Phosphor Screen (GE Healthcare). The screen was scanned using a Storm Image and Detection system (Molecular Dynamics).

Phosphorylated NtrX (NtrX ~ P) was generated as described above, and the phosphorylation mixture was directly added to the binding reaction.

The unlabeled promoters used in the competition assays were generated by PCR using unlabeled nucleotides and were isolated by agarose gels. The bands with the expected molecular weight for each promoter were purified, quantified (Nanodrop, Thermo), and used in the experiments.

DNAse I footprinting

The fragment of pYX used in DNase I footprinting (footprinting probe) was generated as follows: the oligonucleotide 5′-GTCCCATTCATGTCG GTCGT-3′ was 5′ end-labeled with ^{32}P by using [γ-^{32}P]-ATP and T4 polynucleotide kinase (New England Biolabs). The DNA fragment was amplified by PCR using the ^{32}P-labeled primer, primer

5′-AGCACTACAGTTGCATTCTTCG-3′, and genomic DNA from *B. abortus* 2308 as template. The PCR product was then purified on a native polyacrylamide gel. DNase I footprinting experiments were performed with the same binding protocol as in gel shift experiments using 1.2×10^5 cpm of the ^{32}P-labeled probe and 4 μM NtrX. After protein binding, $MgCl_2$ and $CaCl_2$ concentrations were adjusted to 1.5 and 0.5 mM, respectively, and each reaction mixture was incubated with 1 U of RQ1 DNase I (Promega) for 1 min at room temperature. Reactions were stopped by the addition of 5 μl of stop solution (25 mM EDTA and 0.6 M sodium acetate). Digested products were extracted by phenol-chloroform, ethanol precipitated, and resuspended in 4 μl of sequencing gel loading buffer. DNA fragments were then separated on a 6% polyacrylamide DNA sequencing gel. The gel was dried and exposed to a Storage Phosphor Screen (GE Healthcare). The screen was scanned using a Storm Image and Detection system (Molecular Dynamics).

DNA sequencing reactions were carried out with the Sequenase kit version 2.0 (Affymetrix), following the manufacturer's instructions, to localize the position of the protected regions.

In vivo reporter assay

For this assay, two types of plasmids were used. The first one corresponds to a pBBR1MCS-4 vector that has a 4.5-kb fragment that contains a *lacZ* promoter-probe cassette from plasmid pAB200 cloned under the control of the pYX promoter [3], while the other plasmids were pET24 expression vectors with full-length NtrX and the truncated REC domain cloned [3,15]. *E. coli* BL21 pLys were transformed by electroporation with the pBBR plasmid, and one of the expression vectors and the strains with both plasmids were selected based on their resistance to ampicillin and kanamycin. Two colonies from each strain were used to inoculate liquid media supplemented with antibiotics, and all the cultures were grown at 37 °C overnight. Then, they were diluted 1/100 by duplicate with fresh medium and incubated at 37 °C until the optical density reached 0.5. After this time, IPTG (1 mM) was added to one of the tubes of each colony, and all the cultures were incubated for another hour. Finally, the β-galactosidase activity was determined for each one using a standard Miller assay. The reported value corresponds to the average of the two colonies of each strain.

Accession numbers

The coordinates of apo NtrX, and NtrX in complex with ATP and ADP have been deposited in the PDB with accession codes 5M7O, 5M7N, and 5M7P, respectively.

Supplementary data to this article can be found online at http://dx.doi.org/10.1016/j.jmb.2016.12.022.

Acknowledgments

This work was supported by a grant from the Agencia Nacional de Promoción Científica y Tecnológica (ANPCyT, PICT-2013-1629). We also acknowledge access to the X-ray facilities at the ESRF synchrotron (France) and the High Throughput Crystallization Laboratory of the EMBL Grenoble Outstation. M.C.C., R.S., and F.A.G. are researchers from CONICET. I.F. is recipient of a fellowship from CONICET and also earned a fellowship from the Argentinian Ministry of Science and Technology and the EMBL to visit the Grenoble Outstation. We would like to acknowledge support from the European Union through the Seventh Framework Programme grant BioStruct-X (grant agreement No. 283570) and the Horizon 2020 Programme grant iNEXT (grant agreement No. 653706).

Received 31 October 2016;
Received in revised form 21 December 2016;
Accepted 29 December 2016
Available online 12 January 2017

Keywords:
Brucella abortus;
two-component system;
bacterial enhancer binding protein;
NtrY;
transcription factor

†I.F. and I.C. contributed equally to this work.
‡https://embl.fr/htxlab
§https://embl.fr/htxlab
‖http://www.pymol.org

Abbreviations used:
TCS, two-component system; HK, histidine kinase; RR, response regulator; DBD, DNA-binding domain; HTH, helix-turn-helix; bEBP, bacterial enhancer-binding protein; BSA, buried surface area; AcP, acetyl phosphate; SEC, size-exclusion chromatography; SLS, static light scattering; DLS, dynamic light scattering; EMSA, electrophoretic mobility shift assay; FRET, Fluorescence Resonance Energy Transfer; TEV, Tobacco Etch Virus.

References

[1] R. Gao, A.M. Stock, Biological insights from structures of two-component proteins, Annu. Rev. Microbiol. 63 (2009) 133–154, http://dx.doi.org/10.1146/annurev.micro.091208.073214.

[2] S.C. Olsen, M.V. Palmer, Advancement of knowledge of *Brucella* over the past 50 years, Vet. Pathol. 51 (2014) 1076–1089, http://dx.doi.org/10.1177/0300985814540545.
[3] M.D.C. Carrica, I. Fernández, M.A. Martí, G. Paris, F.A. Goldbaum, The NtrY/X two-component system of *Brucella* spp. acts as a redox sensor and regulates the expression of nitrogen respiration enzymes, Mol. Microbiol. 85 (2012) 39–50, http://dx.doi.org/10.1111/j.1365–2958.2012.08095.x.
[4] M.D.C. Carrica, I. Fernández, R. Sieira, G. Paris, F.A. Goldbaum, The two-component systems PrrBA and NtrYX coordinately regulate the adaptation of *Brucella abortus* to an oxygen-limited environment, Mol. Microbiol. 88 (2013) 222–233, http://dx.doi.org/10.1111/mmi.12181.
[5] K. Pawlowski, U. Klosse, F.J. de Bruijn, Characterization of a novel *Azorhizobium caulinodans* ORS571 two-component regulatory system, NtrY/NtrX, involved in nitrogen fixation and metabolism, Mol. Gen. Genet. 231 (1991) 124–138.
[6] Y. Kumagai, Z. Cheng, M. Lin, Y. Rikihisa, Biochemical activities of three pairs of *Ehrlichia chaffeensis* two-component regulatory system proteins involved in inhibition of lysosomal fusion, Infect. Immun. 74 (2006) 5014–5022, http://dx.doi.org/10.1128/IAI.00735-06.
[7] Z. Cheng, M. Lin, Y. Rikihisa, *Ehrlichia chaffeensis* proliferation begins with NtrY/NtrX and PutA/GlnA upregulation and CtrA degradation induced by proline and glutamine uptake, MBio 5 (2014), e02141. http://dx.doi.org/10.1128/mBio.02141-14.
[8] J.M. Atack, Y.N. Srikhanta, K.Y. Djoko, J.P. Welch, N.H.M. Hasri, C.T. Steichen, et al., Characterization of an ntrX mutant of *Neisseria gonorrhoeae* reveals a response regulator that controls expression of respiratory enzymes in oxidase-positive proteobacteria, J. Bacteriol. 195 (2013) 2632–2641, http://dx.doi.org/10.1128/JB.02062-12.
[9] D. Wang, H. Xue, Y. Wang, R. Yin, F. Xie, L. Luo, The *Sinorhizobium meliloti* ntrX gene is involved in succinoglycan production, motility, and symbiotic nodulation on alfalfa, Appl. Environ. Microbiol. 79 (2013) 7150–7159, http://dx.doi.org/10.1128/AEM.02225-13.
[10] J.M. Skerker, M.S. Prasol, B.S. Perchuk, E.G. Biondi, M.T. Laub, Two-component signal transduction pathways regulating growth and cell cycle progression in a bacterium: a system-level analysis, PLoS Biol. 3 (2005), e334. http://dx.doi.org/10.1371/journal.pbio.0030334.
[11] M. Bush, R. Dixon, The role of bacterial enhancer binding proteins as specialized activators of σ54-dependent transcription, Microbiol. Mol. Biol. Rev. 76 (2012) 497–529, http://dx.doi.org/10.1128/MMBR.00006-12.
[12] P.I. Hanson, S.W. Whiteheart, AAA+ proteins: have engine, will work, Nat. Rev. Mol. Cell Biol. 6 (2005) 519–529, http://dx.doi.org/10.1038/nrm1684.
[13] W.C. Bowman, R.G. Kranz, A bacterial ATP-dependent, enhancer binding protein that activates the housekeeping RNA polymerase, Genes Dev. 12 (1998) 1884–1893.
[14] W. Dischert, P.M. Vignais, A. Colbeau, The synthesis of *Rhodobacter capsulatus* HupSL hydrogenase is regulated by the two-component HupT/HupR system, Mol. Microbiol. 34 (1999) 995–1006.
[15] I. Fernández, L.H. Otero, S. Klinke, M.D.C. Carrica, F.A. Goldbaum, Snapshots of conformational changes shed light into the NtrX receiver domain signal transduction mechanism, J. Mol. Biol. 427 (2015) 3258–3272, http://dx.doi.org/10.1016/j.jmb.2015.06.010.
[16] U. Zander, G. Hoffmann, I. Cornaciu, J.-P. Marquette, G. Papp, C. Landret, et al., Automated harvesting and processing of protein crystals through laser photoablation, Acta Crystallogr. D Struct. Biol. 72 (2016) 454–466, http://dx.doi.org/10.1107/S2059798316000954.
[17] L. Aravind, V. Anantharaman, S. Balaji, M.M. Babu, L.M. Iyer, The many faces of the helix-turn-helix domain: transcription regulation and beyond, FEMS Microbiol. Rev. 29 (2005) 231–262, http://dx.doi.org/10.1016/j.femsre.2004.12.008.
[18] N.K. Vidangos, J. Heideker, A. Lyubimov, M. Lamers, Y. Huo, J.G. Pelton, et al., DNA recognition by a σ(54) transcriptional activator from *Aquifex aeolicus*, J. Mol. Biol. 426 (2014) 3553–3568, http://dx.doi.org/10.1016/j.jmb.2014.08.009.
[19] E. Krissinel, K. Henrick, Secondary-structure matching (SSM), a new tool for fast protein structure alignment in three dimensions, Acta Crystallogr. D Biol. Crystallogr. 60 (2004) 2256–2268, http://dx.doi.org/10.1107/S0907444904026460.
[20] S.-Y. Lee, A. De La Torre, D. Yan, S. Kustu, B.T. Nixon, D.E. Wemmer, Regulation of the transcriptional activator NtrC1: structural studies of the regulatory and AAA+ ATPase domains, Genes Dev. 17 (2003) 2552–2563, http://dx.doi.org/10.1101/gad.1125603.
[21] J.D. Batchelor, M. Doucleff, C.-J. Lee, K. Matsubara, S. De Carlo, J. Heideker, et al., Structure and regulatory mechanism of *Aquifex aeolicus* NtrC4: variability and evolution in bacterial transcriptional regulation, J. Mol. Biol. 384 (2008) 1058–1075, http://dx.doi.org/10.1016/j.jmb.2008.10.024.
[22] M.G. Meyer, S. Park, L. Zeringue, M. Staley, M. McKinstry, R.I. Kaufman, et al., A dimeric two-component receiver domain inhibits the sigma54-dependent ATPase in DctD, FASEB J. 15 (2001) 1326–1328.
[23] E. Krissinel, K. Henrick, Inference of macromolecular assemblies from crystalline state, J. Mol. Biol. 372 (2007) 774–797, http://dx.doi.org/10.1016/j.jmb.2007.05.022.
[24] G. Sarkar, I. Edery, N. Sonenberg, Photoaffinity labeling of the cap-binding protein complex with ATP/dATP. Differential labeling of free eukaryotic initiation factor 4A and the eukaryotic initiation factor 4A component of the cap-binding protein complex with [alpha-32P]ATP/dATP, J. Biol. Chem. 260 (1985) 13,831–13,837.
[25] B.E. Aubol, B. Nolen, J. Shaffer, G. Ghosh, J.A. Adams, Novel destabilization of nucleotide binding by the gamma phosphate of ATP in the yeast SR protein kinase Sky1p, Biochemistry 42 (2003) 12,813–12,820, http://dx.doi.org/10.1021/bi035200c.
[26] I. Rombel, P. Peters-Wendisch, A. Mesecar, T. Thorgeirsson, Y.K. Shin, S. Kustu, MgATP binding and hydrolysis determinants of NtrC, a bacterial enhancer-binding protein, J. Bacteriol. 181 (1999) 4628–4638.
[27] N. Joly, J. Schumacher, M. Buck, Heterogeneous nucleotide occupancy stimulates functionality of phage shock protein F, an AAA+ transcriptional activator, J. Biol. Chem. 281 (2006) 34,997–35,007, http://dx.doi.org/10.1074/jbc.M606628200.
[28] D.S. Weiss, J. Batut, K.E. Klose, J. Keener, S. Kustu, The phosphorylated form of the enhancer-binding protein NTRC has an ATPase activity that is essential for activation of transcription, Cell 67 (1991) 155–167.
[29] B.E. Scharf, Summary of useful methods for two-component system research, Curr. Opin. Microbiol. 13 (2010) 246–252, http://dx.doi.org/10.1016/j.mib.2010.01.006.
[30] K.M. Davies, E.D. Lowe, C. Vénien-Bryan, L.N. Johnson, The HupR receiver domain crystal structure in its nonphospho and inhibitory phospho states, J. Mol. Biol. 385 (2009) 51–64, http://dx.doi.org/10.1016/j.jmb.2008.10.027.

[31] M. Rappas, J. Schumacher, H. Niwa, M. Buck, X. Zhang, Structural basis of the nucleotide driven conformational changes in the AAA+ domain of transcription activator PspF, J. Mol. Biol. 357 (2006) 481–492, http://dx.doi.org/10.1016/j.jmb.2005.12.052.

[32] J. Gregor, T. Zeller, A. Balzer, K. Haberzettl, G. Klug, Bacterial regulatory networks include direct contact of response regulator proteins: interaction of RegA and NtrX in *Rhodobacter capsulatus*, J. Mol. Microbiol. Biotechnol. 13 (2007) 126–139, http://dx.doi.org/10.1159/000103604.

[33] L.M. Hellman, M.G. Fried, Electrophoretic mobility shift assay (EMSA) for detecting protein-nucleic acid interactions, Nat. Protoc. 2 (2007) 1849–1861, http://dx.doi.org/10.1038/nprot.2007.249.

[34] S. Park, M. Meyer, A.D. Jones, H.P. Yennawar, N.H. Yennawar, B.T. Nixon, Two-component signaling in the AAA+ ATPase DctD: binding Mg^{2+} and $BeF3^{-}$ selects between alternate dimeric states of the receiver domain, FASEB J. 16 (2002) 1964–1966, http://dx.doi.org/10.1096/fj.02-0395fje.

[35] M. Doucleff, B. Chen, A.E. Maris, D.E. Wemmer, E. Kondrashkina, B.T. Nixon, Negative regulation of AAA + ATPase assembly by two component receiver domains: a transcription activation mechanism that is conserved in mesophilic and extremely hyperthermophilic bacteria, J. Mol. Biol. 353 (2005) 242–255, http://dx.doi.org/10.1016/j.jmb.2005.08.003.

[36] K. Jung, L. Fried, S. Behr, R. Heermann, Histidine kinases and response regulators in networks, Curr. Opin. Microbiol. 15 (2012) 118–124, http://dx.doi.org/10.1016/j.mib.2011.11.009.

[37] K.M. Davies, V. Skamnaki, L.N. Johnson, C. Vénien-Bryan, Structural and functional studies of the response regulator HupR, J. Mol. Biol. 359 (2006) 276–288, http://dx.doi.org/10.1016/j.jmb.2006.02.072.

[38] N. Joly, N. Zhang, M. Buck, X. Zhang, Coupling AAA protein function to regulated gene expression, Biochim. Biophys. Acta 1823 (2012) 108–116, http://dx.doi.org/10.1016/j.bbamcr.2011.08.012.

[39] N. Vidangos, A.E. Maris, A. Young, E. Hong, J.G. Pelton, J.D. Batchelor, et al., Structure, function, and tethering of DNA-binding domains in σ(54) transcriptional activators, Biopolymers 99 (2013) 1082–1096, http://dx.doi.org/10.1002/bip.22333.

[40] A. Narayanan, S. Kumar, A.N. Evrard, L.N. Paul, D.A. Yernool, An asymmetric heterodomain interface stabilizes a response regulator–DNA complex, Nat. Commun. 5 (2014) 3282, http://dx.doi.org/10.1038/ncomms4282.

[41] V. Weiss, F. Claverie-Martin, B. Magasanik, Phosphorylation of nitrogen regulator I of *Escherichia coli* induces strong cooperative binding to DNA essential for activation of transcription, Proc. Natl. Acad. Sci. 89 (1992) 5088–5092.

[42] D. Scholl, B.T. Nixon, Cooperative binding of DctD to the dctA upstream activation sequence of *Rhizobium meliloti* is enhanced in a constitutively active truncated mutant, J. Biol. Chem. 271 (1996) 26,435–26,442.

[43] A. Barnard, A. Wolfe, S. Busby, Regulation at complex bacterial promoters: how bacteria use different promoter organizations to produce different regulatory outcomes, Curr. Opin. Microbiol. 7 (2004) 102–108, http://dx.doi.org/10.1016/j.mib.2004.02.011.

[44] A.E. Maris, M.R. Sawaya, M. Kaczor-Grzeskowiak, M.R. Jarvis, S.M.D. Bearson, M.L. Kopka, et al., Dimerization allows DNA target site recognition by the NarL response regulator, Nat. Struct. Biol. 9 (2002) 771–778, http://dx.doi.org/10.1038/nsb845.

[45] M. Drummond, J. Clements, M. Merrick, R. Dixon, Positive control and autogenous regulation of the nifLA promoter in *Klebsiella pneumoniae*, Nature 301 (1983) 302–307.

[46] A. Alvarez-Morales, R. Dixon, M. Merrick, Positive and negative control of the glnA ntrBC regulon in *Klebsiella pneumoniae*, EMBO J. 3 (1984) 501–507.

[47] A.B. Hervás, I. Canosa, E. Santero, Regulation of glutamate dehydrogenase expression in *Pseudomonas putida* results from its direct repression by NtrC under nitrogen-limiting conditions, Mol. Microbiol. 78 (2010) 305–319, http://dx.doi.org/10.1111/j.1365-2958.2010.07329.x.

[48] J. Pittard, H. Camakaris, J. Yang, The TyrR regulon, Mol. Microbiol. 55 (2005) 16–26, http://dx.doi.org/10.1111/j.1365-2958.2004.04385.x.

[49] H. Liu, T. Von Ohlen, C. Cheng, B. Faburay, R.R. Ganta, Transcription of *Ehrlichia chaffeensis* genes is accomplished by RNA polymerase holoenzyme containing either sigma 32 or sigma 70, PLoS One 8 (2013), e81780. http://dx.doi.org/10.1371/journal.pone.0081780.

[50] T. Unger, Y. Jacobovitch, A. Dantes, R. Bernheim, Y. Peleg, Applications of the restriction free (RF) cloning procedure for molecular manipulations and protein expression, J. Struct. Biol. 172 (2010) 34–44, http://dx.doi.org/10.1016/j.jsb.2010.06.016.

[51] E. Gasteiger, C. Hoogland, A. Gattiker, S. Duvaud, M.R. Wilkins, R.D. Appel, et al., Protein identification and analysis tools on the ExPASy server, In *The Proteomics Protocols Handbook*, Humana Press, Totowa, NJ, 2005: pp. 571–607. doi:10.1385/1-59259-890-0:571.

[52] N. Dimasi, D. Flot, F. Dupeux, J.A. Márquez, Expression, crystallization and X-ray data collection from microcrystals of the extracellular domain of the human inhibitory receptor expressed on myeloid cells IREM-1, Acta Crystallogr. F Struct. Biol. Cryst. Commun. 63 (2007) 204–208, http://dx.doi.org/10.1107/S1744309107004903.

[53] F. Cipriani, M. Röwer, C. Landret, U. Zander, F. Felisaz, J.A. Márquez, CrystalDirect: a new method for automated crystal harvesting based on laser-induced photoablation of thin films, Acta Crystallogr. D Biol. Crystallogr. 68 (2012) 1393–1399, http://dx.doi.org/10.1107/S0907444912031459.

[54] D. de Sanctis, A. Beteva, H. Caserotto, F. Dobias, J. Gabadinho, T. Giraud, et al., ID29: a high-intensity highly automated ESRF beamline for macromolecular crystallography experiments exploiting anomalous scattering, J. Synchrotron Radiat. 19 (2012) 455–461, http://dx.doi.org/10.1107/S0909049512009715.

[55] O. Svensson, S. Malbet-Monaco, A. Popov, D. Nurizzo, M.W. Bowler, Fully automatic characterization and data collection from crystals of biological macromolecules, Acta Crystallogr. D Biol. Crystallogr. 71 (2015) 1757–1767, http://dx.doi.org/10.1107/S1399004715011918.

[56] W. Kabsch, XDS, Acta Crystallogr. D Biol. Crystallogr. 66 (2010) 125–132, http://dx.doi.org/10.1107/S0907444909047337.

[57] G.M. Sheldrick, Experimental phasing with SHELXC/D/E: combining chain tracing with density modification, Acta Crystallogr. D Biol. Crystallogr. 66 (2010) 479–485, http://dx.doi.org/10.1107/S0907444909038360.

[58] K. Cowtan, The Buccaneer software for automated model building. 1. Tracing protein chains, Acta Crystallogr. D Biol. Crystallogr. 62 (2006) 1002–1011, http://dx.doi.org/10.1107/S0907444906022116.

[59] A.J. McCoy, R.W. Grosse-Kunstleve, P.D. Adams, M.D. Winn, L.C. Storoni, R.J. Read, Phaser crystallographic software, J. Appl. Crystallogr. 40 (2007) 658–674, http://dx.doi.org/10.1107/S0021889807021206.

[60] O.S. Smart, T.O. Womack, C. Flensburg, P. Keller, W. Paciorek, A. Sharff, et al., Exploiting structure similarity in refinement: automated NCS and target-structure restraints in BUSTER, Acta Crystallogr. D Biol. Crystallogr. 68 (2012) 368–380, http://dx.doi.org/10.1107/S0907444911056058.

[61] P. Emsley, K. Cowtan, Coot: model-building tools for molecular graphics, Acta Crystallogr. D Biol. Crystallogr. 60 (2004) 2126–2132, http://dx.doi.org/10.1107/S0907444904019158.

[62] G.J. Kleywegt, A.T. Brünger, Checking your imagination: applications of the free *R* value, Structure 4 (1996) 897–904.

[63] V.B. Chen, W.B. Arendall, J.J. Headd, D.A. Keedy, R.M. Immormino, G.J. Kapral, et al., MolProbity: all-atom structure validation for macromolecular crystallography, Acta Crystallogr. D Biol. Crystallogr. 66 (2010) 12–21, http://dx.doi.org/10.1107/S0907444909042073.

[64] F. Sievers, A. Wilm, D. Dineen, T.J. Gibson, K. Karplus, W. Li, et al., Fast, scalable generation of high-quality protein multiple sequence alignments using Clustal Omega, Mol. Syst. Biol. 7 (2011) 539, http://dx.doi.org/10.1038/msb.2011.75.